Addressing of individual atoms in an optical dipole trap

von
Mkrtych Khudaverdyan

Diplomarbeit in Physik

angefertigt im
Institut für Angewandte Physik

vorgelegt der
Mathematisch-Naturwissenschaftlichen Fakultät
der Rheinischen Friedrich-Wilhelms-Universität
Bonn
im November 2003

Referent: Prof. Dr. D. Meschede
Korreferent: Prof. Dr. I.Brock

Contents

Introduction

The field of quantum information processing is rapidly growing and has been attracting a lot of attention within the last decade. Special properties of quantum systems, like interference, entanglement and exponentially scaling state space , open fundamentally new possibilities for storing and processing information. Theoretical studies show that the approach of quantum computation is intrinsically more powerful than the classical one [Sho97].

The experimental realization of systems suitable for quantum computation, however, encounters severe technical difficulties. Several approaches exist, using nuclear spins [Chu98], trapped ions [Mon95, Gul03], quantum dots [San02], superconducting Josephson junctions [Mak01] and cavity quantum electrodynamics. Each of these approaches has its own advantages and disadvantages.

Our approach is to use neutral atoms as carriers of quantum information, which is encoded in their long-living hyperfine ground states. The main advantage of neutral atoms is their weak interaction with the environment and, hence, potentially long coherence times. A chain of noninteracting atoms, prepared in specific quantum states, forms a quantum register. The controlled interaction between two atoms, necessary to perform quantum logic operations can be realized by placing two of them at a time into the mode of a high finesse cavity and by forcing them to controllably share a cavity photon.

A number of necessary steps toward the realization of this scheme have already been accomplished in our group. We use a specially designed magneto optical trap (MOT) [Hau96] as a source of single atoms. In order to store the atoms in a specific quantum state we load them from the MOT into the conservative potential of dipole trap. Using a standing wave dipole trap we can transport atoms over macroscopic distances with submicrometer precision [Kuh01, Sch01b], in order to place them in the cavity mode. While a high finesse cavity has been set up [Mir02, Ros03] and is now in the stage of improvement and optimization, my contribution, presented in this thesis, was focused on the preparation of the atoms

in a quantum register.

Within a chain of stored atoms, each atom can now be addressed individually and coherently manipulated using microwave radiation.

By applying a magnetic field gradient along the dipole trap axis and working with a magnetic field sensitive atomic transition we are able to map the resonance frequency of the atom to its position along the dipole trap axis. During my work, using a recently installed intensified CCD camera, methods were developed to image and spatially resolve the atoms in the dipole trap, and thus to obtain information about their resonance frequency. Applying adiabatic passages, induced by microwave radiation, the inversion of the population of a priori chosen atom was achieved without affecting the population of the other atoms.

Combining the ability to resolve individual atoms within the dipole trap and to induce position-dependent population transfer between hyperfine states of a trapped atoms, we are able now to address an individual atom within an atom chain.

Chapter 1

A source of single neutral atoms

This chapter covers the source of single atoms for our experiments. Two different traps are employed. A magneto-optical trap (MOT) serves as a source of a small and a well-known number of cold cesium atoms. The atoms can be transferred from the MOT into another optical trap - the dipole trap. The purpose of the dipole trap in our experiments is to keep the atoms in a conservative potential in the well-defined electronic state. I start with the description of the basis and experimental setup of the MOT. Then I consider the dipole trap, where I give a short outlook of the origin of the dipole forces and describe the configuration of our dipole trap.

1.1 Magneto-optical trap

For the manipulation of individual neutral atoms it is necessary to have a source of a small number of cold atoms. In this part I describe the principle of operation of a MOT, as well as the concrete realization of the MOT in our experiment.

1.1.1 Principle of operation

The idea of laser cooling of neutral atoms was first considered and proposed by Haensch and Schwalow (1975) [HÄN75] and was later realized independently by Wineland and Dehmelt (1975) [WIN75] for cooling of ions. Later in 1985 Balykin [BAL85] reported on successful transverse laser cooling of atoms in one- and two-dimensions. In the same year Steven Chu realized laser cooling of neutral atoms in three dimensions [CHU85].

Spontaneous scattering force

The near resonant light induces a mechanical effect on the two-level atom. Consider two-level atom interacting with a laser beam. Absorbtion of a photon from the

laser field results in an absorbtion of the momentum $\hbar\mathbf{k}$, where $\mathbf{k}$ is the wave vector with the absolute value of $k = 2\pi/\lambda$. The succeeding emission of a photon can be stimulated by the laser field (induced emission) or occur spontaneously. In the first case the momentum of the emitted photon is equal to the momentum of the previously absorbed photon and the net momentum transfer is zero. As opposed to the stimulated emission, spontaneous emission has no preferred direction in free space, and the average momentum carried away in this process is zero, whereas a momenta of the photons, absorbed from the laser, add up collinearly and increase the momentum transfer to the atom. This results in a pushing force along the direction of laser beam propagation. This type of mechanical effect of the laser beam on the atom is known as light pressure or *spontaneous scattering force*.

Doppler cooling

Laser cooling relies on the fact that scattering of photons from the near-resonant light field by an atoms is strongly frequency dependent. The velocity of an atom results in a Doppler frequency shift of atomic transition with respect to the radiation field frequency. This results in a velocity dependent absorbtion of the light and can be used to slow an atom. In order to qualitatively understand the damping of an atomic velocity in the field of red-detuned counter-propagating laser beams, we first consider a simplified one-dimensional case, where the momenta of the atom and photons lie along one axis.

In the reference frame of the moving with the velocity v atom, the frequency of the counter-propagating beam is shifted closer to the atomic resonance by $\Delta\omega_{\text{Dop}} = \omega v/c$, while the detuning of the co-propagating laser beam becomes larger. Hence the atom absorbs more photons, arriving from the direction opposite to its motion and thus the residual force experienced by the atom is always opposed to its velocity and vanishes if the atom is stationary. The resulting mechanism of damping of the atomic velocity, based on the Doppler effect, is called *Doppler cooling*.

The radiation pressure force, averaged over many absorbtion and emission processes, in the case of two counter-propagating laser beams of the small intensity is equal to [MET99], (see Fig. 1.1):

$$\mathbf{F}_{\text{tot}} = \mathbf{F}_+ + \mathbf{F}_- \tag{1.1}$$

where

$$\mathbf{F}_\pm = \pm\frac{\hbar\mathbf{k}\Gamma s_0}{2(1 + s_0 + (2(\delta \mp \Delta\omega_{\text{Dop}})/\Gamma)^2}. \tag{1.2}$$

Here, s_0 is the resonance saturation parameter, Γ is the natural linewidth of the atomic transition and the detuning δ is a difference of the frequencies of the atomic transition and the laser field $\delta = \omega - \omega_0$. This force reaches its maximum when the Doppler effect brings the moving atom in resonance with the counter-propagating laser beam (see Fig 1.1). Hence, the velocity capture range is defined by the detuning of the laser field with respect to the atomic resonance. For small v from (1.1) follows that the net force is proportional to the velocity:

$$\mathbf{F} = -\alpha\mathbf{v}, \tag{1.3}$$

and acts as a friction force. Thus this configuration of counter-propagating laser beams is referred as an *optical molasses*, where atoms are slowed down by the laser field.
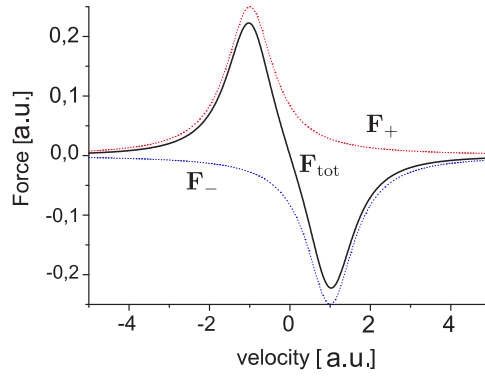
Figure 1.1: velocity dependence of radiation damping force for one-dimensional optical molasses.$\mathbf{F}_-$ and $\mathbf{F}_+$ show the force from each beam, $\mathbf{F}_{\mathrm{tot}}$ is their sum.

However, in reality $v = 0$ cannot be achieved. The minimum velocity is determined by the equilibrium between heating and cooling processes. The origin of the heating lies in statistical fluctuations of the radiation pressure force. This fluctuations come from random directions of spontaneously emitted photon momenta.

It was demonstrated that the theoretical minimum velocity using this cooling mechanism is achievable at a red detuning, which equals to the half of the natural linewidth [LET77]:

$$v_D = \sqrt{\frac{\hbar\Gamma}{m_{\mathrm{Cs}}}} \tag{1.4}$$

This velocity is called Doppler velocity and for cesium it is about 9 cm/s. Slowed atoms undergo spatial random walks inside the optical molasses and eventually

escape the molasses. To avoid this an additional position-dependent force has to be introduced.

Position-dependent force

For a simpler explanation of the localization mechanism consider an atom having an optical transition between $F = 0$ and $F = 1$ levels in the presence of red-detuned counter-propagating laser beams with σ^+ and σ^+ polarizations, respectively (see Fig. 1.2 a)). In the presence of a linear gradient magnetic field, the degeneracy of the excited state $F = 1$ is lifted and the splitting of Zeeman sublevels raises linearly with the distance from the magnetic zero-point. This forms a one dimensional MOT.

Stationary atom displaced to the left (right) from the zero-point of the magnetic field scatters more photons from the σ^+ (σ^-) laser beam and is pushed back to the magnetic field zero point. Hence the atom is always pushed towards the center of the MOT.
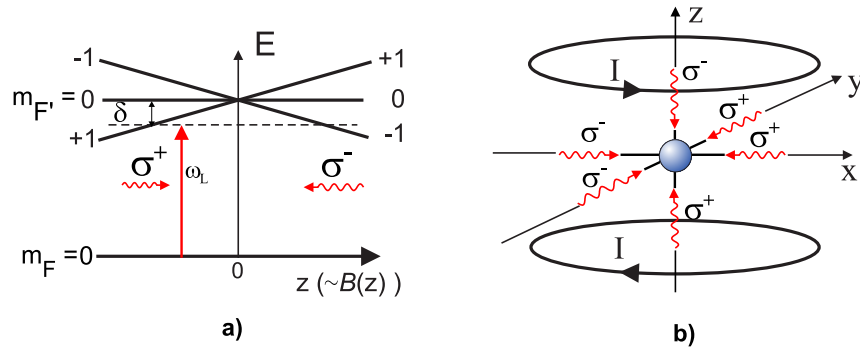
Figure 1.2: Magneto-optical trapping of the atom in: a) one dimension b) in all three dimension. The magnetic field lifts the degeneracy of the excited state. The atom experiences the restoring force as long as it moves away from the trap center.

To cool atoms down in all three direction one uses three orthogonal pairs of counter-propagating red-detuned laser beams, which form a three dimensional optical molasses. Overlapping it with the quadrupole magnetic field, which varies linearly in all directions from the magnetic field zero-point [MET99, PET02]:

$$B = B'(x^2 + y^2 + 4z^2)^{\frac{1}{2}}, \tag{1.5}$$

one can generalize the described cooling and trapping mechanism for all three dimensions (see Fig. 1.2 b)).

1.1.2   Experimental realization

In our experiment we use a high gradient MOT as a source of single or few Cs atoms. The high gradient reduces the capture cross section of the MOT and allows us to work on the level of single or very small number of atoms.

To cool Cs atoms we use the $|F = 4\rangle \longrightarrow |F' = 5\rangle$ transition (see Fig. 1.3). With a small but finite probability an atom can be off-resonantly excited by the cooling laser to the $F' = 4$ state, and can decay into $F = 3$. To bring the atom back into the cooling cycle we use an additional repumping laser, which is resonant with the $|F = 3\rangle \rightarrow |F' = 4\rangle$ transition.
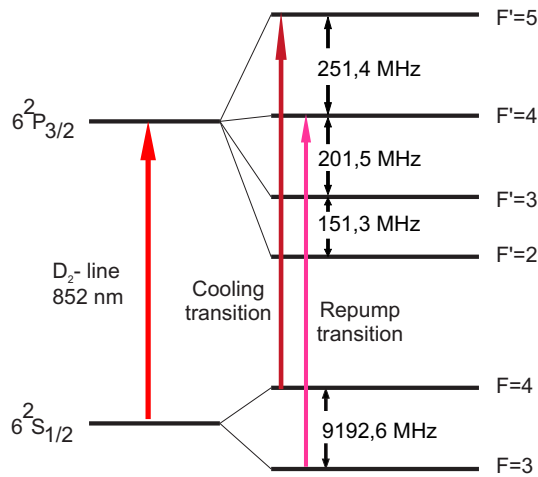
Figure 1.3: Level scheme of the D2-line of Cs.

The schematic view of the MOT setup is presented in Fig. 1.4. The magnetic coils in anti-Helmholtz configuration produce a quadrupole magnetic field with 160 G/cm in the x-y plane at the center of the MOT.

The fluorescence light from the MOT is collected and collimated by a home made diffraction limited objective (NA= 0.29) [ALT03]. The light is spatially and spectrally filtered before it is focused onto an avalanche photodiode (APD). The quantum efficiency of the APD is around 50 % at the Cesium wavelength of λ =852 nm. The exact number of atoms can be determined at any time within 10 ms using the signal from the APD.

A typical fluorescence signal from the MOT is presented in Fig. 1.5. Each atom contributes by the same amount to the total fluorescence signal. The steps in the

(a)
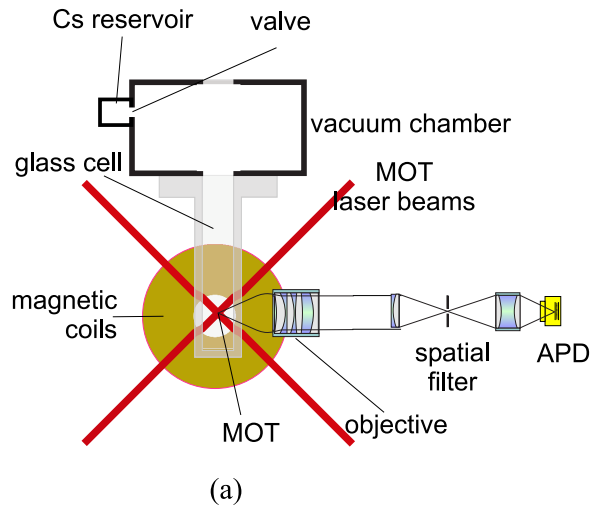
Figure 1.4: The MOT setup and the imaging optics. Fluorescence light is collected by imaging optics and is detected by the APD.

florescence signal correspond to the capture or loss of atoms. Magnetic coils in an
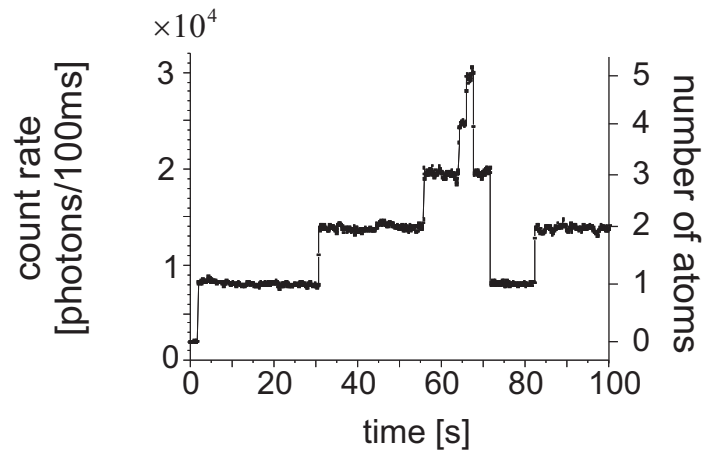
Figure 1.5: The fluorescence light collected by the imaging optics and detected by the APD proportional to the number of atoms trapped in the MOT. By monitoring the fluorescence signal one can directly infer number of atoms trapped inside the MOT.

anti-Helmholtz configuration impose the quadrupole magnetic field.

1.2   Dipole trap

Apart from the MOT, we have an additional dipole trap. In contrast to the MOT, the dipole trap imposes a conservative potential to the atoms. Due to its long coherence time [KUH03], the dipole trap can be used to store atoms in a specific quantum state. The dipole trap can serve as a conveyor belt for single atoms [SCH01B, KUH01] to transport them along the dipole trap axis.

In this part I discuss the principle of the dipole force, the experimental realization of the dipole trap and of the conveyor belt.

1.2.1   Dipole force

The idea of dipole force was first theoretically considered by Askaryan (1962) [ASK62] in connection to plasmas and neutral atoms. The dipole force acting on neutral atoms was first demonstrated by Bjorkholm (1978) [BJO78], and later Chu (1986) [CHU86] was the first to exploit this force to realize a dipole trap for neutral atoms.

In contrast to the strongly dissipative radiation pressure force in the MOT, the dipole force imposes a conservative potential, and arises due to dispersive interaction of the induced atomic dipole moment with the laser field intensity gradient.

In a classical picture (Lorentz model) an atom is considered as a charged harmonic oscillator which interacts with a classical radiation field. In this model an electron is considered to be bound to the core elastically and oscillates at a frequency ω_0.

The dipole moment of the atom in an external field $\boldsymbol{E}(t) = \boldsymbol{E}e^{i\omega t}$ + c. c., can be expressed in the following form $\boldsymbol{p}(t) = e\boldsymbol{x}(t) = \boldsymbol{p}e^{i\omega t}$+c.c. $= \alpha\boldsymbol{E}(t)$, where e is the charge of the oscillator and α is the polarizability. α can be found by integrating the following equation of motion $\ddot{\boldsymbol{x}}(t) + \Gamma\dot{\boldsymbol{x}}(t) + \omega_0^2\boldsymbol{x}(t) = e/m_{\mathrm{e}}\boldsymbol{E}(t)$:

$$\alpha = \frac{e^2}{m_{\mathrm{e}}}\frac{1}{\omega_0^2 + \omega^2 - i\omega\Gamma}. \tag{1.6}$$

Here Γ is a damping rate due to the radiative energy loss [JAC62]. The interaction energy of the dipole moment $\boldsymbol{p}(t)$ driven by external electromagnetic field $\boldsymbol{E}(t)$ is $U_{\mathrm{int}} = -\frac{1}{2}\boldsymbol{p}(t)\cdot\boldsymbol{E}(t)$. After time averaging over the rapid oscillation the interaction potential takes the following form [GRI00]:

$$U_{\mathrm{dip}}(r) = \mathrm{Re}(\alpha)\boldsymbol{E}(t)^2 = -\frac{1}{2\epsilon_0 c}\mathrm{Re}(\alpha)I \sim 1/\Delta, \tag{1.7}$$

where I is the field intensity and Δ is the detuning $\Delta = \omega_0 - \omega$. Taking the gradient of (1.7), the dipole force reads:

$$\boldsymbol{F}_{\text{dip}}(\vec{r}) = -\vec{\nabla}(U_{\text{dip}}) = -\frac{1}{2\epsilon_0 c}\text{Re}(\alpha)\vec{\nabla}I \tag{1.8}$$

Hence, the dipole interaction energy is proportional to the in-phase component of the induced dipole moment. This fact explains the dispersive nature of the dipole force.

Re(α) as a function of detuning $\Delta = \omega - \omega_0$ has a dispersive shape (see Fig. 1.6). The sign of the detuning determines whether an atom is pushed by the dipole force to the region of the high or low field intensity. Indeed, for the red-detuned field the dipole potential is negative and, thus, an atom is attracted to regions of the high intensity, whereas for the blue-detuned field an atom is pushed out of the intensity maximum.

The oscillator absorbs power from the external field:

$$P = \langle \dot{\boldsymbol{p}}\boldsymbol{E} \rangle = \frac{\omega}{c\epsilon_0}\text{Im}(\alpha)I, \tag{1.9}$$

where $\langle ... \rangle$ is a time average. This power is then emitted by the atom as a sequence of quanta of energy $\hbar\omega_0$, resulting in the atomic scattering rate:

$$\Gamma_{\text{sc}} = \frac{1}{2\epsilon_0 c\hbar}\text{Im}(\alpha)I \sim 1/\Delta^2. \tag{1.10}$$

Because the scattering rate scales as $1/\Delta^2$ and potential depth as $1/\Delta$, it is preferably to have a high field intensity and a large detuning to reduce the scattering rate for a fixed potential depth.

1.2.2 Standing wave dipole trap

Our dipole trap is generated by two counter-propagating Gaussian laser beams of equal intensities, frequencies and parallel linear polarizations [SCH00]. Due to interference, two counter-propagating laser beams result in a standing wave interference pattern of the intensity, which in turn yields a periodic potential with the periodicity $\lambda/2$, where $\lambda = 1064\ nm$. So, our dipole trap potential has the following form in cylindrical coordinates:

$$U(\rho, z) = U_0\,\frac{w_0^2}{w^2(z)}\,e^{-\frac{2\rho^2}{w^2(z)}}\,\cos^2(kz), \tag{1.11}$$
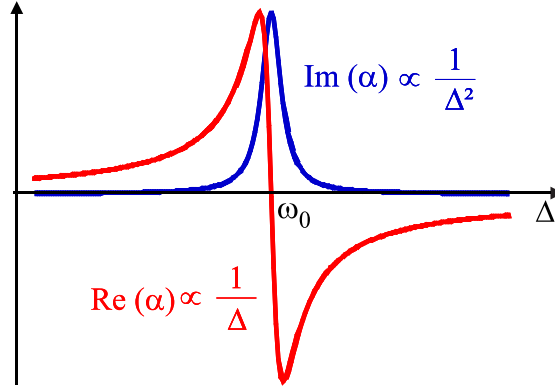
Figure 1.6: Imaginary and real part of α. The dipole force is proportional to the real part of α. The scattering rate is proportional to the imaginary part of the α.

where

$$k = 2\pi/\lambda$$

is the optical wavevector. The $1/e^2$ radius $w(z)$ of the beam is given by

$$w^2(z) = w_0^2 \left(1 + \frac{z^2}{z_R^2} \right),$$

w_0 is the beam waist and $z_R = \pi w_0^2/\lambda$ the Rayleigh length.
Since the detuning of the Nd:YAG laser is much larger than the fine structure splitting of Cs states $6^2 P_{1/2}$ and $6^2 P_{3/2}$, the depth of the dipole trap is given by:

$$U_0 = \frac{\hbar \Gamma}{2} \frac{P}{\pi w_0^2 I_0} \frac{\Gamma}{\Delta_{\text{eff}}}. \tag{1.12}$$

Here, P is the total power of both beams. I_0 is the saturation intensity, Γ is the natural linewidth, and Δ_{eff} is an effective laser detuning:

$$\frac{1}{\Delta_{\text{eff}}} = \frac{1}{3} \left(\frac{2}{\Delta_{3/2}} + \frac{1}{\Delta_{1/2}} \right). \tag{1.13}$$

Effective detuning includes contribution from both D-1 ($\Delta_{1/2}$) and D2 ($\Delta_{3/2}$) transitions of Cs [GRI00]. The scattering rate is given by

$$\Gamma_{sc}(\mathbf{r}) = \frac{\Gamma}{8} \frac{I(\mathbf{r})}{I_0} \left(\frac{\Gamma}{\Delta_{\text{eff}}} \right)^2. \tag{1.14}$$

In our case the depth of the dipole trap is about 2.9 mK at the total power of 2.6 W and the waist $2w_0 = 16$ μm and the scattering rate is about 10 photons/s^{-1}, which makes heating due to spontaneous scattering force negligible.

1.3 Transfer of atoms between MOT and dipole trap

The general procedure for all of our experiments is the following. Initially, we prepare an exactly known number of atoms in the MOT. Then we transfer them into the dipole trap, where we perform some intermediate experiments with the trapped atoms. Then we transfer the atoms back into the MOT. Then by looking at their fluorescence signal, we define their number. So we use the MOT as an atom counter. 100% transfer efficiency between the MOT and the dipole trap allows us to define initial number of atoms in the intermediate experiments and their number after performing intermediate experiments.

In order to transfer the atoms from the MOT into the dipole trap, both traps are overlapped for several milliseconds - the beams of the standing wave dipole trap are focused at the position of the MOT (see Fig. 1.8). The necessary requirement for having high transfer efficiency is that the depth of the dipole trap is bigger than the kinetic energy of the atoms. Typically, in our experiments the depth of the dipole trap is by a factor of 10 bigger than the atomic kinetic energy during the transfer, and we can achieve the transfer efficiency close to 100 %.

A typical transfer procedure is sketched in Fig. 1.7
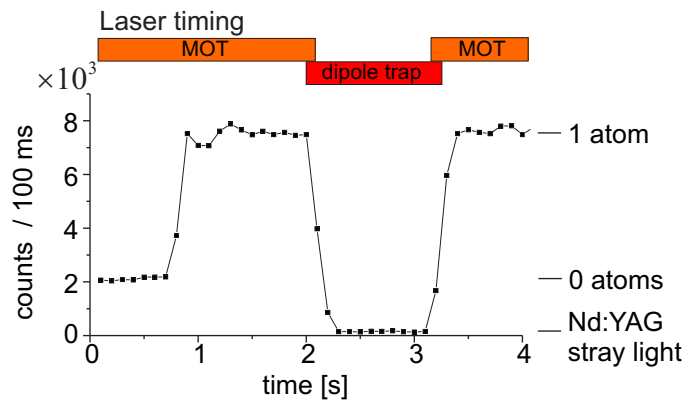
**Figure 1.7**: The fluorescence light collected by the APD during the atom transfer between the MOT and the dipole trap. The atom is transferred from the MOT to the dipole trap, stays there for about 1 s, and is transferred back into the MOT.

In this figure one sees, that the experiment starts with no atoms in the MOT. After around 1 s one atom is loaded into the MOT. Then the traps are overlapped by

several milliseconds and the MOT is switched off. The atom in the dipole trap does not fluoresce. Then we apply the reversed procedure to reload the atom back into the MOT. After that, by looking at the fluorescence signal from the MOT, we see whether the atom is lost or not.

To carry out experiments with atoms in the dipole trap, it is important to have a low atomic loss rate from this trap. The typical lifetime of an atom in our dipole trap is about 20 sec [ALT03]. The main limitation of the lifetime is imposed by collisions with a background gas [ALT03].

1.4   Conveyer belt for single neutral atoms

An atom, initially trapped in a stationary dipole trap, can be brought into motion along the optical axis mutually detuning the frequencies of the counter-propagating laser beams.

This results in a position and time-dependent potential:

$$U(\rho, z, t) = U_0 \, \frac{w_0^2}{w^2(z)} \, e^{-\frac{2\rho^2}{w^2(z)}} \, \cos^2(\pi\delta\nu t - kz), \tag{1.15}$$

Changing the detuning $\delta\nu$ results in a movement of the standing-wave pattern with the velocity $v = \delta\nu\lambda/2$. In order to realize the conveyer belt experimentally we use the AOMs (see Fig. 1.8) to detune the frequencies of counter-propagating laser beams. Initially stationary dipole trap is accelerated by a linear ramp of the mutual frequency difference of both AOMs. Any noise of the relative phase of the AOMs results in a spatial fluctuation of the dipole trap and leads to the heating of stored atoms. It therefore can cause an eventual escape out of the trap. To avoid this destruction effect we detune the frequencies of the AOMs in a phase-continuous way.
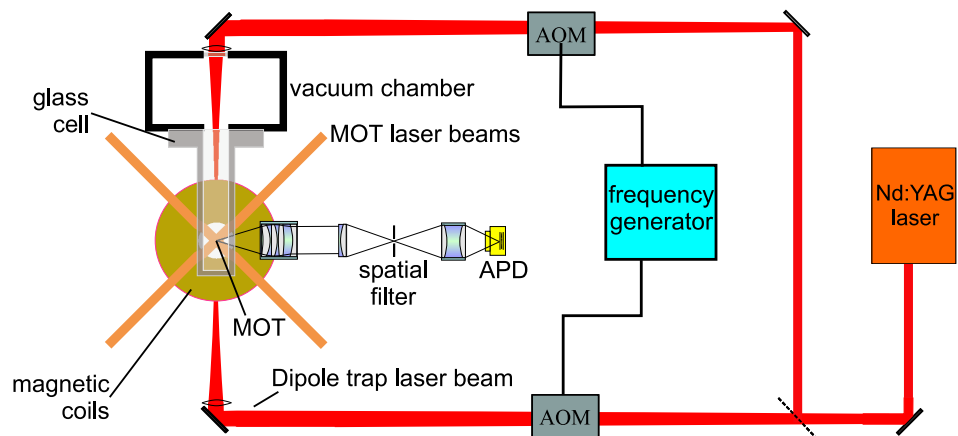
Figure 1.8: Sketch of the dipole trap setup. We operate the dipole trap as an optical conveyor belt by mutual detuning the frequencies of the dipole trap laser beams using the AOMs.

Chapter 2

Resolving single neutral atoms

In this chapter I present the continuous imaging of individual atoms in an optical dipole trap. The observation of a single atom in an optical dipole trap has already been realized in the group of P. Grangier, where single atoms leave and enter the dipole trap statistically several times during the exposure [SCH01A]. We have accomplished to non-destructively observe one and the same atom for one minute.

Whereas non-destructive observation of single atoms in the MOT allows us to measure their spatial distribution in this trap, the ability to resolve single neutral atoms within the dipole trap forms the basis to manipulate the trapped atoms individually.

2.1   Imaging optics

The main part of the imaging optics was covered in Chapter 1. Here I will concentrate on the description of the intensified CCD camera (ICCD). It allows us to obtain information about the spatial position of trapped atoms. The fluorescence light from the MOT is collected by the objective with $f = 36$ mm, collimated and evenly splitted by a beam splitter. The light, which is reflected from the beam splitter is focused with a lens of $f = 500$ mm onto the photocathode of the ICCD camera (see Fig. 2.1). Thus, the imaging optics has a magnification of 14, and one pixel (13μm$\times13\mu$m) on the CCD array corresponds to 0.93 μm at a MOT cite. The FWHM of the point spread function of our imaging optics is equal to 1.4 μm and the focus depth is equal to 7.4 μm. Below the characterization of this ICCD camera is described.
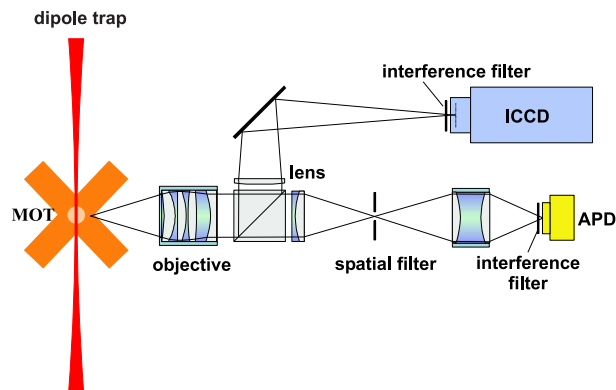
Figure 2.1: Scheme of the experimental setup. The fluorescence light from the MOT is collimated and divided into two parts by the beam splitter. One part is sent onto the APD, while the other part is imaged onto the intensified CCD camera.

2.2 Intensified CCD camera

In order to observe a single trapped atom within a short time, a camera with high quantum efficiency and noise to signal ratio is required.

2.2.1 Principle of CCD camera

Our high-resolution CCD camera (Roper Scientific, PI-MAX, 1024×1024 pixel) consists of an intensifier (GEN III, Roper Scientific), which is fiber-optically coupled to the CCD array. This ICCD can be controlled externally - it can be triggered to start an exposure and a corresponding exposure time can be controlled. The exposure time for a single image can be varied between few nanoseconds to several minutes. The intensifier is sketched in Fig. 2.2. Basically, it is a high-voltage vacuum tube, consisting of the photocathode on the inside of the input window and the phosphor screen on the output window. Photoelectron, released from the photocathode gets amplified by the electron-multiplying micro channel plate (MCP). The back surface of the MCP is attached to the phosphor screen, which is connected to the CCD array by a fiber-optic bundle.

Step by step, an incident photon is converted to a fluorescence burst on the phosphor screen [PRI]:

1) Incident photon passes through the intensifier input window, strikes the photocathode, and releases a photoelectron. The probability for the electron to be ejected is defined by the quantum efficiency (QE). It is the GaAs coating which
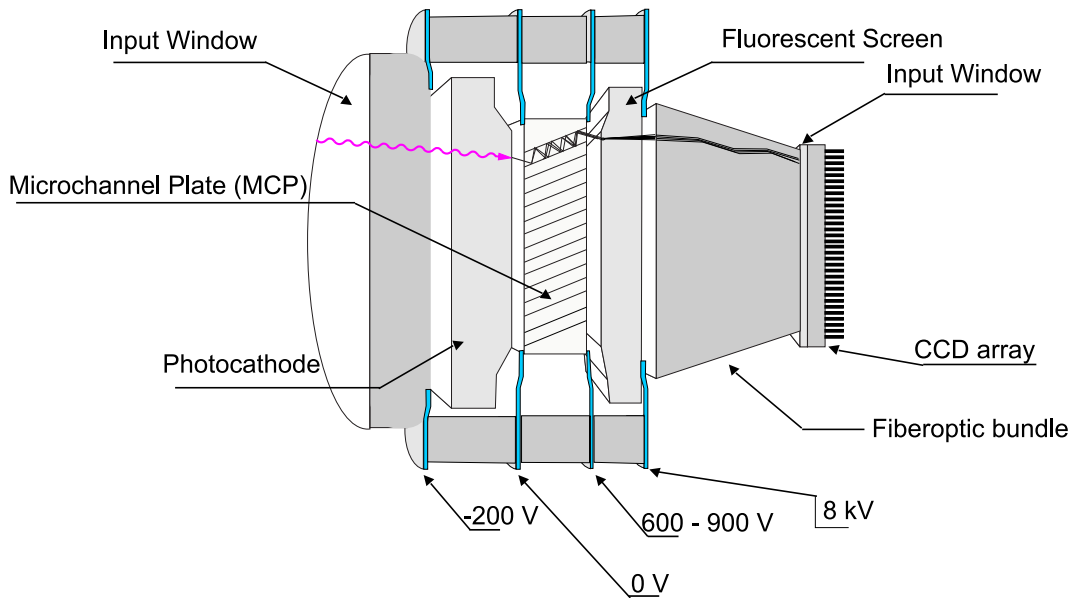
Figure 2.2: Major components of the intensified CCD camera.

provides a high QE of the photocathode in the visible, and what is important for the purposes of our experiment, in a near infrared region.

Ionized gases, present in the vacuum tube are accelerated towards the photocathode and can thus destroy the coating. In order to avoid this deterioration, a thin film of metal oxide is applied to the input metal surface of the MCP. This film is only partially transparent for the incident photoelectrons. The net QE, which includes loss mechanisms on both photocathode and the film, is specified to be 30 % at the wavelength of $\lambda =852$ nm. The measured QE is turn out to be smaller by a factor of 3. The measurement of QE was performed by comparing the number of photons, detected by the APD and ICCD within the same time interval, provided the QE of APD is 50%.

2) The electrons, ejected from the photocathode are then accelerated across a half millimeter gap towards a MCP. It is a slightly conductive glass substrate with millions of parallel traversing channels, containing a secondary electron emitter on their inner walls. A portion of the electrons, passing through the MCP strike its walls, causing the formation of secondary electrons. This collision takes place multiple times, resulting in a generation of several thousands of electrons at the output. By tuning the voltage of the MCP output, the amplification gain can be adjusted. Furthermore, electronic *Gating* is controlled by the sign of the voltage on

the MCP.

3) The electrons, exiting the MCP are further accelerated by a constant high voltage (5-8 kV) and strike the phosphor screen, converting their kinetic energy into the release of photons.

4) The photons, released by the phosphor screen are coupled to a CCD array by the fiberoptic bundle and produce counts (charges) at the pixel they strike. According to the specification the transmission of the fiberoptic bundle is as high as 40 %.

5) After the image is acquired, the accumulated charge in the CCD array is shifted to the serial register, that converts the charge to an analog voltage. This signal is then sent to a special converter, which digitizes a signal and sends it to the interface card, installed on the host computer.

2.2.2 Characterization of the intensified CCD camera

A single photon without being amplified normally generates a number of counts in the CCD array which is smaller than the noise, generated in the same array. In contrast, with insertion of an intesifier a single photon signal exceeds the noise level by far. However, the intensifier produces noises on the CCD array. I will discuss the main noise sources in the following:

Intensifier noise

a) Statistical noise

Statistical noise stands for the uncertainty in the number of counts on the CCD array, produced by a single photoelectron. Hence it limits the precision of attributing the number of detected photons, provided the number of counts generated in the CCD is known. The emission of a photoelectron from the photocathode is a probabilistic event, governed by the binomial statistics. As the electron strikes the MCP, the number of secondary electrons N fluctuates around its average value with an amplitude of $\sqrt{N}$, which is the result of the Poissonian statistics. The same happens at each amplification stage. Hence, the overall number of counts acquired by the CCD pixel from one photoelectron is governed by the product of the Poissonian distributions. Below, in Fig. 2.3 the measured distribution of the number of counts, generated by a single photoelectron is presented. From this distribution we determine, that a single photoelectron produces 350 counts on average. This measurement was performed with the closed camera and switched on intensifier, so that only randomly emitted thermal photoelectrons were detected.
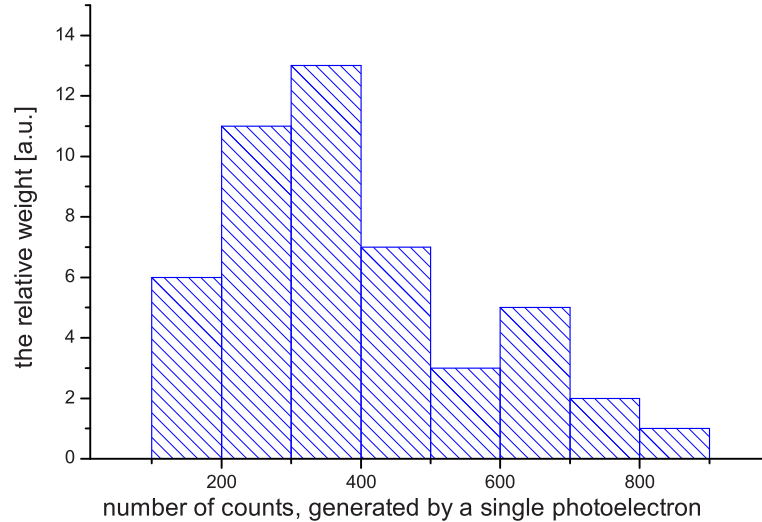
Figure 2.3: The histogram of the number of counts, generated on the CCD array
by a single photoelectron, emitted from the photocathode.

b) Equivalent background illumination (EBI)

This part of the noise in an intensifier comes from thermal electrons, released from
the photocathode. Such an electron generates a similar number of counts on the
CCD as a photoelectron ejected by the incident on the photocathode photon. These
thermal electrons generates a background of 5.4 counts per pixel per second, which
correspond to approximately 16200 ejected photoelectrons. Note, that the counts
are not homogeneously distributed over the CCD array.

Noises on the CCD-chip

The noise on the CCD array itself can be divided into two components — the readout
noise and the dark current noise. The readout produces an offset of about 80-90
counts per pixel per read out with an rms-fluctuations of 9 counts per pixel. The
dark current noise is one count per pixel per second and is therefore negligible.

Stray-light background

Stray light further reduces the signal to noise ratio. For the standard powers of
the laser beams and normal illumination in the laboratory an average number of

"stray" photons, detected by the photocathode within 1 s is approximately equal to 385×10^3, which corresponds to 0.37 photons per pixel per second.

2.2.3 Single photon on the CCD

For each photoelectron the multichannel plate together with the fluorescence screen produce a burst of photons. This burst, incident on the CCD chip, generates counts in a 3×3 pixel area. About 50 % of the counts are concentrated in a central pixel, the other half is distributed among the surrounding 8 pixels. A typical distribution of the counts on the CCD array, produced by a single photoelectron is depicted in Fig. 2.4. Here 5×5 pixel area on CCD array is depicted, containing counts, produced by a single photoelectron. The FWHM of the counts distribution is determined by binning the pixels of the depicted area in X-direction and fitting the resulting histogram with a Gaussian. A large statistics of the counts distribution were fitted, and the resulting FWHM determined to be 2.3±0.13 pixels.
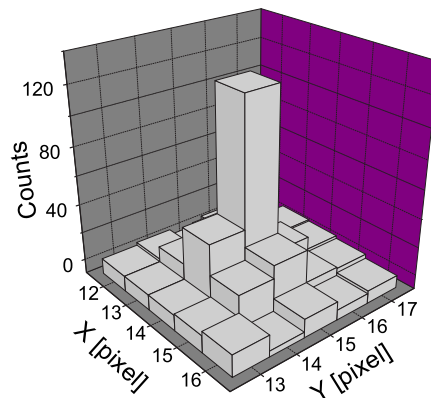
Figure 2.4: Pixel distribution of the photon burst on the CCD chip, generated by a single photoelectron. The counts are distributed over a 3×3 pixel area (on this image [13-15,14-16] in X-Y coordinates). The counts are subtracted by the read out counts.

2.3 Continuous imaging of trapped atoms

Imaging atoms in the MOT

The image of a single atom stored in the MOT is presented in Fig. 2.5. In this case the exposure time was 1 sec. Within this time interval the fluorescence light

of a single atom in the MOT generates approximately 6400 photoelectrons on the photocathode of the ICCD camera. The spatial distribution of the atom, confined in the MOT can be extracted from this picture. This is accomplished by binning the pixels of the image in vertical and horizontal directions and fitting the resulting histogram with a Gaussian. From this image one can see that the atom is confined within a volume in space with the horizontal and vertical sizes of 11 μm and 13 μm, respectively.
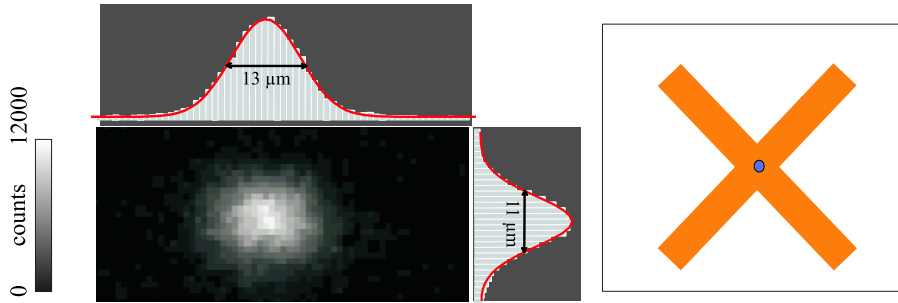
Figure 2.5: Image of one atom stored in the MOT. Exposure time is 1 s. To determine the size and the absolute position of the spacial distribution of a single atom, stored in the MOT, the counts are binned in the vertical and horizontal directions and fitted with Gaussians.

Illumination of atoms in the dipole trap

In order to extract information about the spatial position of the atoms inside the dipole trap, imaging method have to be developed. Atoms, stored in the far red-detuned dipole trap do not fluoresce light (see Chapter 1), and thus can not be detected. In order to observe atoms stored in the dipole trap with our ICCD camera we illuminate them with three-dimensional optical molasses (OM), generated by the laser beams of the MOT. This illumination has two different functions - on the one hand it forces atoms to scatter photons, which allows us to detect them, and on the other hand it provides cooling, so that atom stays in the same potential well during the illumination.

The cooling performance of the OM crucially depends on three parameters - detuning and intensity of the illuminating laser beams and the potential depth of the dipole trap, determined by the intensity of the trapping laser beams. Optimal parameters are found experimentally. The regular procedure for this purpose is the following: we first load a number of atoms in the MOT and transfer them into the dipole trap. Then we acquire a sequence of images of the atoms, being

illuminated by the OM. The exposure time for each image is 0.5 s with a time interval between succeeding images of 0.3 s. For not optimized illumination parameters the atoms are heated up and, as the result, we observe that the atoms change their position in the dipole trap from image to image or even escape the trap after short time. In contrast, for optimal parameters of OM the atoms are continuously cooled and stay in the same dipole trap potential well without getting lost. As the result, in the sequence of succeeding images atomic position will not change. In this case the lifetime of the atom, stored in the dipole trap is equal to some tens of seconds, and is limited by the collisions with the background gas only.

The optimal power of the dipole trap laser beams is found to be 1.3 W per laser beam with the waist of $2w_0 = 32$ μm. This results in 12 Γ light shift of the atomic cooling transition. The optimal detuning of the cooling laser beam from the cooling transition of a free atom approximately equals to 1.5 Γ. Each OM laser beam is focused to a waist of $2w_0 = 2$ mm and has 100 μW power. This corresponds to 13.5 Γ detuning of the cooling laser beam from the light-shifted cooling transition, and the saturation parameter of 0.004 for each OM beam.

Imaging of a single atom in the dipole trap

Figure 2.6 presents the image of a single atom confined in a potential well of the dipole trap and illuminated by OM. The exposure time is 0.5 s.

The width of a single potential well in the radial direction is defined by the waist ($2w_0 = 32$ μm) of dipole trap laser beam. From this image we see that the observed FWHM in radial direction is equal to 7.3 μm. This means that the atom stays close to the bottom of the potential well and thus remains cold during the illumination. The axial width of a single potential well (see Chapter 1) approximately equals to 500 μm. Consequently, we expect the axial spatial width of the image to be of the order of 100 μm. However, the observed axial width of the fluorescence spot is 2.7 μm. There are two main contributions to the observed spread. The width of the point spread function of the imaging optics equals to 1.4 μm. In addition, the width of the counts distribution on the CCD chip, produced by a single photoelectron equals to 2.3 μm. Thus, we can resolve two atoms, which are more than 2.7 μm apart.

Imaging single atoms in the dipole trap we can determine the absolute position of the trapped atom with submicrometer precision. For this purpose we bin the counts in the radial direction and fit the resulting histogram with the Gaussian. The fit error is about 200 nm. This accuracy assumes that the potential well remains at the same position. However, due to the drifts of the dipole trap the accuracy of the
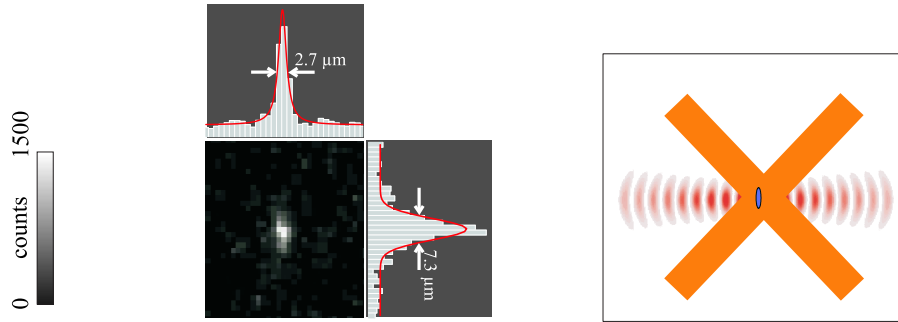
Figure 2.6: Image of one atom, confined in a potential well of the DT and illuminated by the laser beams of an optical molasses (Exposure time 0.5 s).

determined position of the atom is limited to about 400 nm. In order to measure this value we collected a large sequence of images of the same atom, stored in the dipole trap. The exposure time for each image is 0.5 s and the time interval between succeeding images is 0.3 s. Then each image was fitted with the Gaussian, as it was described above, and the rms deviation was calculated.

2.3.1   Observation of a controlled motion of individual atoms

The combination of the ability to perform deterministic transport of single atoms [Kuh01, Sch01b] with the possibility to observe a single atom enable as to perform a continued imaging of single atom controlled motion.

The procedure for this continuous observation is as follows (see Fig. 2.7): we load one atom from the MOT into the dipole trap. Then we switch on the the OM and take the first image of trapped atom. Exposure time equals to 1 s. Then trapped atom is transported with an optical conveyor belt (see Sec. 1.4) to the left over 2 μm distance within 2 ms time. Then the second image is acquired of the trapped atom for 1 s. This procedure is repeated some tens number of times and using our ICCD this controlled motion of the individual atoms is observed. After some tens of seconds the atom is lost from the dipole trap due to the collision with the background gas. Several images out of the sequence are presented in Fig 2.8
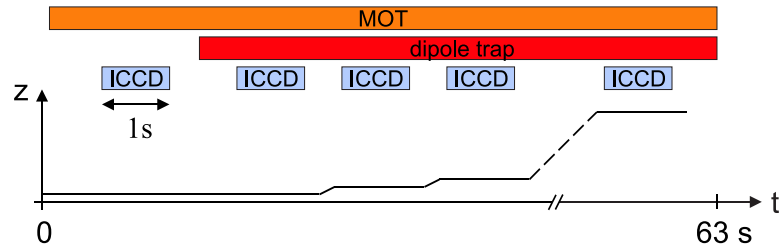
**Figure 2.7**: Transportation of a single atom. After each transportation, trapped atom is illuminate by the OM and the camera picture is taken.
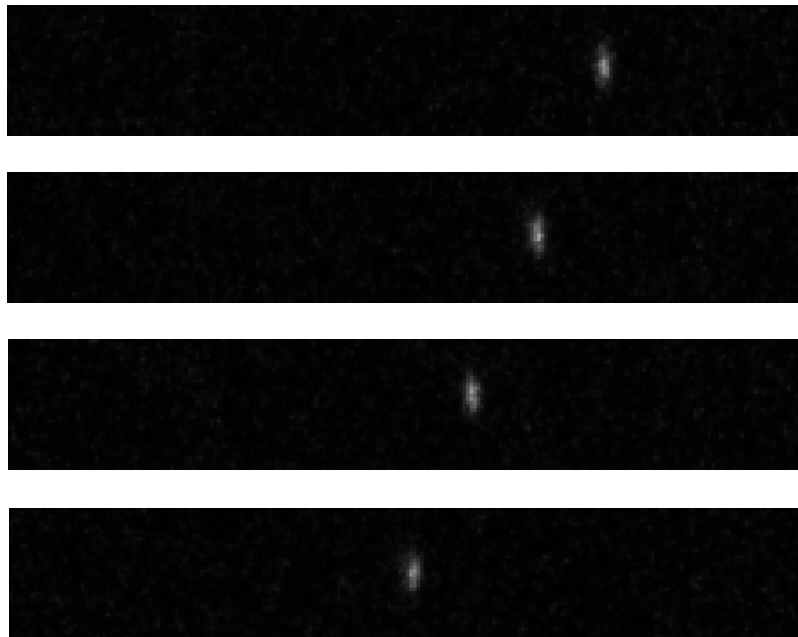

Figure 2.8: Observation of a transportation of a single atom. The atom is transported to the left over 2 μm after each image is acquired. The time interval between the succeeding images is 1.3 s. 1st, 9th, 17th and 25th images are presented.

Chapter 3

Adiabatic passages

There exist different techniques to achieve efficient population transfer in two-level systems. It can be achieved by placing a two-level atom in external coherent resonant field. Such electromagnetic field induces Rabi oscillations between ground and excited states of a two-level atom (in the absence of spontaneous emission) [ALL75, LOU83]. For an interaction time of half a Rabi period, complete population transfer from the ground to the excited state can be achieved. As a necessary requirement for this method to work - one must match the resonance frequency of the corresponding transition and the duration of a corresponding interaction.

As an alternative, there exists a different method of population transfer with an efficiency close to 100%, which is called adiabatic passage. This technique is based on the fact, that if we slowly tune the frequency of the external field, so that it crosses the atomic resonance, population of an atom is transferred from the ground to the excited state. The main advantage of the use of adiabatic passages for the purposes of population transfer, as opposed to those of resonant pulses, is their robustness with respect to fluctuations of the amplitude and the frequency of the external field. In fact, the exact knowledge of the resonant frequency is not required, and efficient population transfer can be achieved for a certain range of the resonance frequencies. The investigation and characterization of this adiabatic population transfer via microwave radiation is the subject of this chapter.

3.1   Theoretical Introduction

In what follows I will only consider the case of a two-level atom. Two different descriptions of adiabatic passages will be described below. First, I will employ Bloch vector formalism to characterize the mechanism and properties of adiabatic passages. As an alternative, we will consider adiabatic passages in the frame of the

dressed state picture.

3.1.1 Coherent population transfer in the Bloch vector model

To describe adiabatic passage transfer between the states of a two-level system it is rather convenient to implement Bloch vector formalism, which allows a geometrical interpretation of the passage. Bloch equations describe the evolution of a state of a two-level atom in an external classical monochromatic electromagnetic field. The Bloch model, as opposed to the dressed state picture does not consider the evolution of the common system of atom and field, but rather treats the evolution of the atomic state alone. It describes the evolution of the atomic density matrix, which in this model couples to the incident field.

The Hamiltonian of a two-level system, interacting with a classical incident field is $\hat{H} = \hat{H}_A + \hat{\mu} \cdot \hat{B}$. Here $\hat{H}_A$ is the Hamiltonian of the free atom, $\hat{\mu}$ is the magnetic moment of the atom and $\hat{B} = B_0 cos(\vec{k}\vec{x} + \omega t)$ is the magnetic part of the external radiation field. The evolution equation for the density matrix $\hat{\rho}$ has the following form ([BOH86]):

$$i\hbar \, \dot{\hat{\rho}} = [\hat{H}, \hat{\rho}] \tag{3.1}$$

Here the density matrix $\hat{\rho}$ is:

$$\hat{\rho} = \begin{pmatrix} \rho_{gg} & \rho_{ge} \\ \rho_{eg} & \rho_{ee} \end{pmatrix}, \tag{3.2}$$

where $|g\rangle$ and $|e\rangle$ are the ground and the excited states of an atom, respectively. The explicit equation for each component of the density matrix is available in the standard textbooks (see [COH92, ALL75]) and won't be considered here.

The rotating wave approximation reflects the fact that we can neglect quickly-rotating terms (at twice the transition frequency), arising in explicit form of (3.2) with respect to those that are evolving at the detuning $\delta = \omega - \omega_0$ of the frequency of the external field from the transition frequency of the two-level atom.

Physically it means that we neglect the following virtual processes:

- Atom in the excited state absorbs a photon and returns in the ground state.

- Atom rises from ground to the excited state by emitting a photon.

Those processes lead to the so-called Bloch-Siegert shift and will not be considered here. This effect is negligible in near-resonant case where the detuning is smaller

than the transition frequency $\delta \ll \omega_0$. The explicit form of (3.1) simplifies even further if we consider (3.2) in the reference frame, rotating at the frequency of the external radiation field:

$$\tilde{\rho}_{ee} = \hat{\rho}_{ee} \tag{3.3a}$$
$$\tilde{\rho}_{gg} = \hat{\rho}_{gg} \tag{3.3b}$$
$$\tilde{\rho}_{ge} = \hat{\rho}_{ge}e^{i\omega t} \tag{3.3c}$$
$$\tilde{\rho}_{eg} = \hat{\rho}_{eg}e^{-i\omega t} \tag{3.3d}$$

The rotating-wave approximation along with (3.3) lead to the following set of equations which are called optical Bloch equations:

$$\dot{\hat{\rho}}_{ee} = i\frac{\Omega}{2}(\hat{\rho}_{eg} - \hat{\rho}_{ge}) \tag{3.4a}$$

$$\dot{\hat{\rho}}_{gg} = i\frac{\Omega}{2}(\hat{\rho}_{ge} - \hat{\rho}_{eg}) \tag{3.4b}$$

$$\dot{\hat{\rho}}_{ge} = -i\frac{\Omega}{2}(\hat{\rho}_{ee} - \hat{\rho}_{gg}) - i\delta\hat{\rho}_{ge} \tag{3.4c}$$

$$\dot{\hat{\rho}}_{eg} = i\frac{\Omega}{2}(\hat{\rho}_{ee} - \hat{\rho}_{gg}) + i\delta\hat{\rho}_{eg} \tag{3.4d}$$

Here Ω is a real-valued and positive physical value, called the Rabi frequency, which reflects the strength of the coherent coupling of the states $|g\rangle$ and $|e\rangle$: $\hbar\Omega = \langle e|\hat{\mu}\hat{B}|g\rangle$.

Furthermore, rewriting (3.4) in the terms of the following set of variables simplifies this equation to the form, allowing a geometrical interpretation:

$$u = (\hat{\rho}_{eg} + \hat{\rho}_{ge}) \tag{3.5a}$$
$$w = (\hat{\rho}_{ee} - \hat{\rho}_{gg}) \tag{3.5b}$$
$$v = (\hat{\rho}_{ge} - \hat{\rho}_{ge}) \tag{3.5c}$$

In the basis of the variables (3.4) reads as follows:

$$\dot{u} = \delta v \tag{3.6a}$$
$$\dot{v} = -\delta u - \Omega w \tag{3.6b}$$
$$\dot{w} = \Omega v \tag{3.6c}$$

This set of equations can be written in the form of a single vector equation:

$$\dot{\boldsymbol{u}} = [\boldsymbol{\Omega}_{\text{eff}} \times \boldsymbol{u}]. \tag{3.7}$$

Here, the torque vector $\mathbf{\Omega}_{\text{eff}} = (\Omega, 0, -\delta)$ and the Bloch vector $\mathbf{u} = (u, v, w)$. Equation (3.7) has a geometrical interpretation: the Bloch vector $\mathbf{u}$ precesses about the torque vector $\mathbf{\Omega}_{\text{eff}}$ at the frequency $|\mathbf{\Omega}_{\text{eff}}| = \sqrt{\Omega^2 + \delta^2}$ (see Fig. 3.1.1). The first, dispersive component of the $\mathbf{u}$, u is in phase with radiation field. The second component v is in quadrature with the external electromagnetic field, and is responsible for the absorption of the energy from the field. Absorption of energy by an atom results in turn in the change of its population and w. The third component w is called inversion and equal to the population difference of the excited and ground states. It is equal to -1 when the atom is in the ground state and equals to 1 when it is excited.
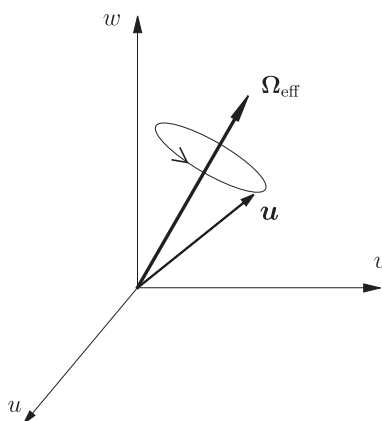
Figure 3.1: Precession of the Bloch vector around the torque vector.

π-pulse

If a two level atom coherently interacts with a resonant electro-magnetic field the population will undergo Rabi oscillations at the Rabi frequency Ω [Lou83]. It can be visualized, using (3.7) and considering the evolution of $\mathbf{u}$ in the Bloch sphere. The resonant radiation of a constant amplitude corresponds to the torque vector $\mathbf{\Omega}_{\text{eff}} = (\Omega, 0, 0)$. On the Bloch sphere it is pointing along the u axis (see Fig. 3.1.1). Consider an atom in the ground state, $\mathbf{u}=(0,0,-1)$. At $t = 0$ we switch on the resonant external field. The Bloch vector starts to precess around $\mathbf{\Omega}_{\text{eff}}$ in the $v - w$ plane at the frequency Ω (see Fig. 3.1.1). After the time $t_\pi = 1/(2\Omega)$, corresponding to the half of a precession period, the Bloch vector will be pointing upwards, corresponding to the excited state of the atom, $\mathbf{u}=(0,0,1)$.

Note that the transfer efficiency equal to 100% is achieved here, provided that radiation field is in resonance with an atom. In the non-resonant case, $\mathbf{\Omega}_{\text{eff}}$ is not

directed parallel to the u axis and the Bloch vector does not precess in the $u - v$ plane. As a consequence, the efficiency of the population transfer drops.
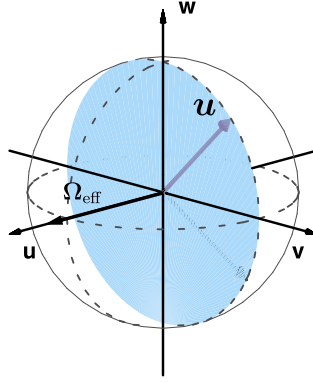
**Figure 3.2**: Precession of the Bloch vector in the $u - v$ plane. The inversion w periodically oscillates between -1 and $+1$, corresponding to the ground and excited states of the atom.

adiabatic following

Here I will describe how we can transfer the atomic population with an efficiency close to 100%, even if the atomic resonance frequency is not exactly known. I will consider the response of the atom to an off-resonant coherent external field, while its frequency is swept across the resonance slowly.

Consider an atom being in its ground state ($w =$-1). An external radiation field has a fixed amplitude and a frequency, slowly and monotonously changing from far red detuning to far blue detuning. The Bloch vector, initially parallel to the torque vector, precesses around the torque vector and follows its direction, if the torque vector changes its direction much more slowly, than the precession period $1/|\mathbf{\Omega_{eff}}|$. Thus at the end of the passage the Bloch vector is parallel to the torque vector and the population inversion is achieved, as long as the detuning crosses zero.

In an experiment the frequency sweep cannot be infinitely large. Since the opening angle between $\mathbf{\Omega_{eff}}$ and $\boldsymbol{u}$ at the beginning of the interaction should be zero and at the end of the passage the torque vector has to point upwards, an appropriate form of the Rabi frequency is required. Since the Rabi frequency is proportional to the square root of the microwave intensity $I^{1/2}$, we can influence the Rabi frequency by changing I. The setting of Rabi frequency to zero at the beginning and at the end of the interaction insures the appropriate direction of the torque vector at

those moments (see Fig. 3.3). Since we want the change of the torque vector to be smooth, Rabi frequency should vary smoothly.

Generally, the Bloch vector u follows Ω_{eff} if the the condition of adiabaticity is satisfied - the change of the Bloch vector direction is smaller than the precession frequency of the Bloch vector about Ω_{eff}. If it is the case, the Bloch vector u remains almost parallel and hence reverse its direction during the passage (see Fig. 3.3).
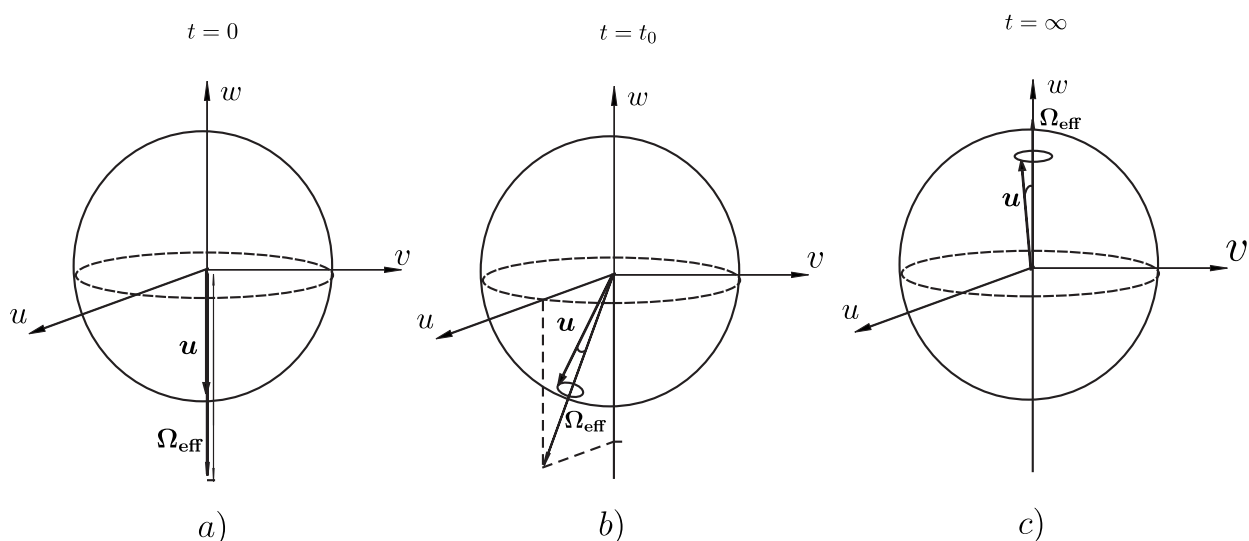
Figure 3.3: Precession of the Bloch vector u about the torque vector Ω_{eff}. a) at time equal $t = 0$ the Bloch vector is exactly parallel to Ω_{eff}, b) at time $t = t_0$ if the requirement of the adiabatic following is fulfilled, the angle α remains very small, c) at time $t = \infty$ the bloch vector is directed almost parallel to the w-axis and the efficiency of the adiabatic passage is almost 100%.

3.1.2 Adiabatic passages in a dressed state picture

adiabatic following

As an alternative to the Bloch vector model I will consider the adiabatic transfer in the dressed state picture. As opposed to the Bloch vector picture, it describes the dynamics of the atom-radiation system as an evolution of its total wave function [GRI73, SHO90]. The adiabatic theorem states that by changing the Hamiltonian quite slowly the system will follow the instantaneous eigenstate [MES65]. I will show, that by choosing an appropriate form of interaction the system will follow a

single eigenstate, which continuously connects the ground and excited atomic states.

Let us consider the Hamiltonian, describing the state of the two-level atom and nearly-monochromatic quantized radiation. In the basis of unperturbed states it has the following form:

$$\hat{H}(t) = \frac{\hbar}{2} \begin{pmatrix} 0 & \Omega(t) \\ \Omega(t) & -2\delta(t) \end{pmatrix}. \tag{3.8}$$

The unperturbed states of the atom and field system are $|g, n+1\rangle$ - state of the atom and field system, where the atom is in its ground state and the field contains $n+1$ photons, and $|e, n\rangle$ - where the atom is in the excited state and there are n photons in the field. The off-diagonal element $\Omega(t)$ is the Rabi frequency. The eigenvalues of this Hamiltonian are:

$$E_\pm = \frac{\hbar}{2} \left(\delta(t) \pm \sqrt{\delta^2(t) + \Omega^2(t)} \right) \tag{3.9}$$

$$E_+ - E_- = \hbar\sqrt{\delta^2(t) + \Omega^2(t)} = \hbar\Omega_{\text{eff}} \tag{3.10}$$

and the corresponding eigenstates are:

$$|a(n)\rangle = \sin(\theta)|g, n+1\rangle + \cos(\theta)|e, n\rangle \tag{3.11}$$

$$|b(n)\rangle = \cos(\theta)|g, n+1\rangle - \sin(\theta)|e, n\rangle, \tag{3.12}$$

$$\tag{3.13}$$

where the mixing angle θ is obtained from the following expression:

$$\tan(2\theta) = -\frac{\Omega(t)}{\delta(t)} \qquad 0 \leq 2\theta < \pi \tag{3.14}$$

The energies of these eigenstates are therefore split by the effective Rabi frequency Ω_{eff}. In Fig. 3.4 the energies of the dressed states presented as a functions of the detuning. Whereas the energies of the unperturbed states intersect at $\delta = 0$, the energies of corresponding dressed states split by the Rabi frequency Ω, which prevents them from mixing. This is called an avoided crossing.

Let us first consider the case of constant detuning. When the interaction strength is equal to zero ($\Omega = 0$) the dressed state coincides with the unperturbed state. Without loss of generality, suppose $\delta < 0$ and $|b(n)\rangle = |g, n+1\rangle$ ($\theta = 0$). By increasing slowly the interaction strength from zero to some intermediate maximum, the state $|b(n)\rangle$ evolves into some mixture of the $|g, n+1\rangle$ and $|e, n\rangle$ states. Decreasing slowly Ω back to zero leads to the return to the state $|g, n+1\rangle$, and no

population transfer is achieved.

A different situation occurs, if we, in addition, sweep slowly the frequency of the radiation field from a very large negative value of the detuning($\delta < 0$ and $|\delta| \gg \Omega$) to a very large positive value ($\delta > 0$ and $|\delta| \gg \Omega$) (or vise versa). Then the system, starts from the ground state, which is in addition equal to dressed state $|b(n)\rangle$ ($\theta = 0$) (see Fig. 3.4). If we slowly sweep the detuning, adiabatically increasing the interaction strength, the system follows the state $|b(n)\rangle$. At the end of the interaction the ratio $\delta/\Omega \longrightarrow -\infty$ and the mixing angle $\theta \longrightarrow \pi/2$. Hence, during the interaction the mixing angle θ rotates from zero to $\pi/2$, and the system, initially being in the ground state, follows the state $|b(n)\rangle$, and ends up in the excited state $|e, n\rangle$ (see (3.11)).

Condition of adiabatic following

The Schroedinger equation for the wave-function Ψ, describing the state of atom-radiation system, written in the basis of dressed states has the following form:

$$i\hbar \frac{d}{dt}\Psi(t) = i\hbar \frac{d}{dt}\begin{pmatrix} c_a(t) \\ c_b(t) \end{pmatrix} = \frac{\hbar}{2}\begin{pmatrix} \Omega_{\text{eff}} & 2i\dot{\theta} \\ -2i\dot{\theta} & -\Omega_{\text{eff}} \end{pmatrix}\begin{pmatrix} c_a(t) \\ c_b(t) \end{pmatrix} \tag{3.15}$$

Here $\Psi = c_a|a(n)\rangle + c_b|b(n)\rangle$. The condition of the adiabatic following requires that the system, initially prepared in $\Psi(t = 0) = |b(n)\rangle$ follows this state and remains in this state after the passage. This requirement means that the coupling between the dressed states remains negligible during the passage. Using (3.15) this condition of adiabaticity can be derived. If the off-diagonal term $2i\dot{\theta}$ were not there, there would not be any coupling between the coefficients c_a and c_b. In this case c_b will be equal to initial value (i.e. $c_b(0)=1$) apart from the phase factor, and c_a will stay zero:

$$c_b(t) = c_b(0)\exp(\int_0^t \frac{i}{2}\Omega_{\text{eff}}(t')dt') \tag{3.16}$$

$$c_a(t) = c_a(0) \equiv 0 \tag{3.17}$$

The off-diagonal element $2i\dot{\theta}$ can be neglected, provided that $\dot{\theta}$ is much smaller than the effective Rabi frequency Ω_{eff}. Using (3.14), one can rewrite the condition of adiabatic following explicitly in terms of Rabi frequency and the detuning:

$$\dot{\theta} = \frac{1}{2}\frac{|\dot{\delta}\,\Omega - \dot{\Omega}\,\delta|}{\delta^2 + \Omega^2} \ll \Omega_{\text{eff}} \tag{3.18}$$

or

$$f(t) = \frac{1}{2}\frac{|\dot{\delta}\,\Omega - \dot{\Omega}\,\delta|}{(\delta^2 + \Omega^2)^{\frac{3}{2}}} \ll 1, \tag{3.19}$$

where $f(t)$ is called adiabaticity function ([Ric00]), which is the measure of the adiabaticity of the passage. From the above given expression one can see, that in order to keep this function small several requirement should be fulfilled. First of all, it is necessary to have a long interaction duration and smooth δ and Ω, which would reduce the time derivatives in the numerator. It also necessary to have large Rabi frequency and the detuning, which reduces the dominator with respect to numenator.
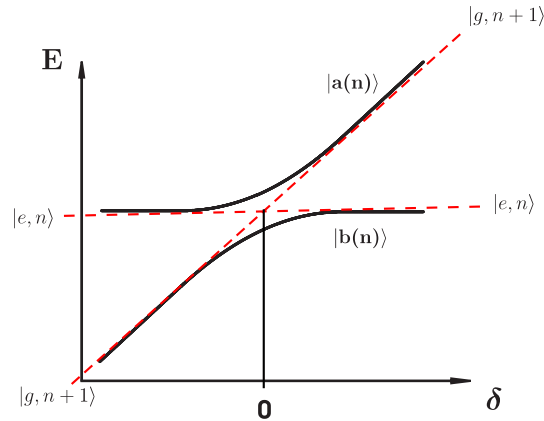
Figure 3.4: Energies of the dressed states $|a(n)\rangle$ and $|b(n)\rangle$ versus detuning δ. A single dressed state connects two different unperturbed states.

3.2   Numerical simulation

In order to demonstrate the mechanism of the adiabatic passage, qualitative description of the adiabatic passage is considered in the previous section.

It is of particular interest to know how the system would respond to the variations of Hamiltonian, if those variation would occur not infinitely slowly. In this section I will concentrate on the application of the adiabatic processes - numerically simulating the adiabatic passage, using certain shape of δ and Ω. Experimentally, the shape of the Ω is controlled by the radiation intensity I, since $\Omega \sim \sqrt{I}$.

In a real experiment one cannot choose an ideal long pulse to induce an efficient population transfer. Usually, and in particularly in our experiment, the limitation on the pulse duration is dictated by the coherence times [Kuh03]. Hence it is necessary to find a special form for Ω and δ, so that still for the pulses of relatively short duration the condition of the adiabatic following will be satisfied.

3.2.1 The chirped microwave pulse

In order to simulate the adiabatic passages, we modulated the amplitude and the frequency of the microwave radiation in such a way, that Ω and δ have the following shape [GUE02]:

$$\Omega(t) = \Omega_{\mathrm{m}} \sin^2\left(t\,\frac{\pi}{t_0}\right) \qquad (3.20)$$

$$\delta(t) = \delta_0 - \delta_{\mathrm{m}} \cos\left(t\,\frac{\pi}{t_0}\right) \qquad (3.21)$$

Here t_0 is the duration of the interaction, Ω_{m} and δ_{m} are the amplitudes of the Rabi frequency and detuning respectively. δ_0 is a constant, which defines the frequency chirp offset with respect to the atomic resonance.

For fixed duration of the interaction those forms of δ and Ω are one of the most optimal for satisfaction of the adiabaticity condition (3.18). The dependency of Ω and δ on time is presented in Fig. 3.5.
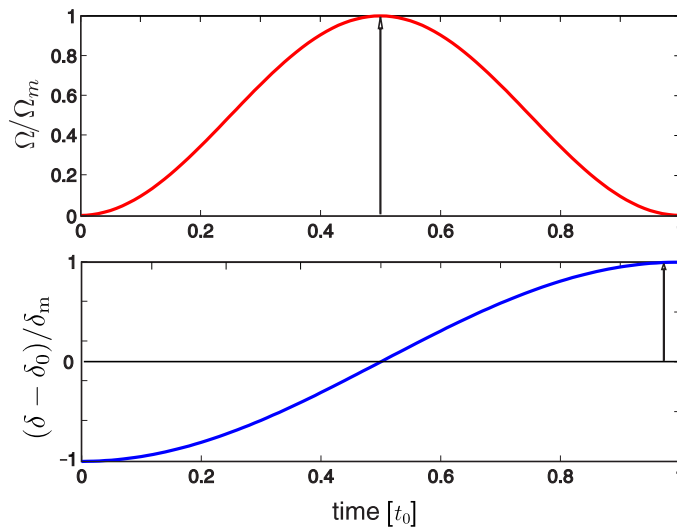

Figure 3.5: The time dependence shape of the Rabi frequency $\Omega(t)$ and the detuning $\delta(t)$, chosen for numerical simulation.

3.2.2 Simulation of adiabatic passage

In order to study the properties of the adiabatic passage it is reasonable to consider the case, where the resonance frequency of the two-level atom is a constant during

population inversion.

In order to numerically calculate the efficiency of the adiabatic passages with the above specified pulses the following steps were taken:

$\Omega(t)$ and $\delta(t)$ (3.20) are inserted into the simplified optical Bloch equations (see Eq. 3.6) and the system of the linear differential equations is integrated over the pulse duration. The frequency chirp offset δ_0 is stepped over the frequency range of about $2\delta_m$, symmetrical with respect to zero. For each δ_0 the third component of the bloch vector w is calculated in the end of the passage, which is the measure of the atomic population after the interaction time. As it was pointed out in Sec. 3.1.1, for slow adiabatic change of Hamiltonian the population inversion will take place as long as the detuning crosses the atomic resonance. This implies, that the population transfer as a function of δ_0 has a plateau-like form with the width of around $2\delta_m$.

As an example let us consider the numerically calculated population transfer for the following set of experimental parameters:

$$
\begin{aligned}
\Omega_{\mathrm{m}} &= 2\pi \times 13.5 \text{ kHz} \\
\delta_{\mathrm{m}} &= 140 \text{ kHz} \\
t_0 &= 2 \text{ ms}
\end{aligned}
\qquad (3.22)
$$

The above specified value of Ω_{m} is limited by the maximal intensity we can generate at the site of the MOT. The pulse duration t_0 has to different limitations. On the one hand it is chosen to be smaller than the coherence time which is of the order of some tens of milliseconds ([KUH03]). On the other the duration should be large enough for the Bloch vector to follow $\mathbf{\Omega_{eff}}$ and to ensure adiabaticity during the interaction. The dependency of the population transfer on δ_0 for the parameters specified above is presented in Fig. 3.6.

The depicted dependency has a plateau-like form and the efficiency of the population transfer reaches 100% over the expected width of about $2\delta_{\mathrm{m}}$. The efficiency drops at $|\delta_0| = \delta_m$ and is equal to zero for larger $|\delta_0|$. In this case the frequency of the external radiation does not cross resonance, and the torque vector as well as the Bloch vector, stay in the lower hemisphere during the interaction so that population transfer does not take place. One also sees that the plateau is not exactly $2\delta_{\mathrm{m}}$ wide and drops within several tens of kHz. This is because the condition of adiabaticity is no longer fulfilled on the edges of the spectrum.

Using $\delta(t)$ and $\Omega(t)$ (3.20) and the set of parameters (4.4) the adiabaticity function $f(t)$ (3.19) was calculated for each moment of the passage and each δ_0. It is
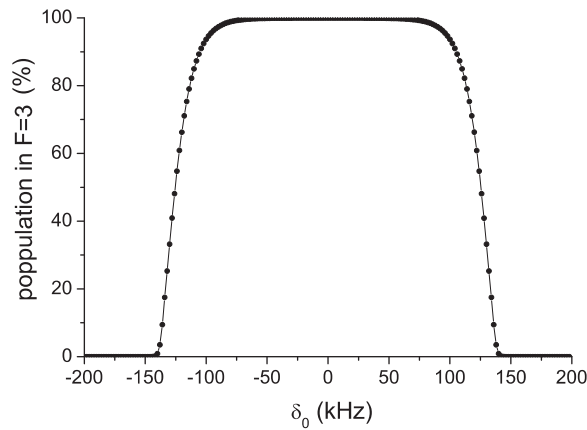
Figure 3.6: The population transfer versus the frequency chirp offset δ_0 for the set of parameters (4.4). Simulated efficiency of population transfer has a plateau-like form with an approximate width of $2\delta_m$.

depicted in Fig. 3.7. The range of δ_0 shown in this figure, is $[-120, 120]$ kHz.
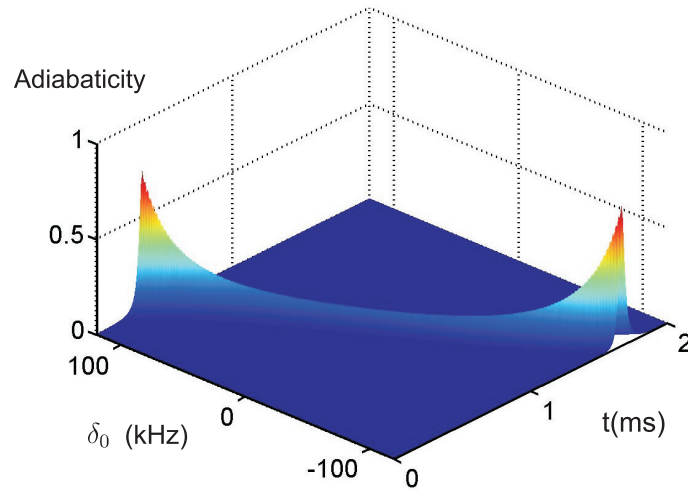
Figure 3.7: The adiabaticity function is plotted versus detuning and time for the pulse given by (3.20) and specified parameters (4.4). The condition of the adiabaticity is no longer fulfilled as long as $|\delta_0|$ approaches δ_m.

From this figure one can see, that for a fixed δ_0, the adiabaticity function reaches its

maximum during the passage in the vicinity of an anticrossing time t_A. t_A is defined as a time, when the frequency of the external field equals to the atomic resonance frequency ($\delta = 0$). For example, for $\delta_0 = 0$ the adiabaticity function reaches its maximum at time $t = t_0/2$. When $|\delta_0|$ increases the adiabaticity function at time t_A also increases. If $|\delta_0|$ approaches δ_m adiabaticity function becomes larger than 1 and the transfer efficiency decreases. As it increases further and exceeds the range $[-\delta_m, \delta_m]$, the adiabatic condition is fulfilled again, but since the detuning does not cross resonance, the population remains in the ground state after the passage.

3.3   Experimental results

In this section I will present the experimental application of the adiabatic passage technique to transfer population between hyperfine ground state of the Cs atoms. The measured spectra agree well with the numerical simulations.

Our two-level system is Zeeman sublevels of the the $6S_{1/2}^2$ hyperfine energy level of Cs - $|F = 4, m_F = 4\rangle$ and $|F = 3, m_F = 3\rangle$, separated by well-known clock transition of 9.2 GHz.

3.3.1   Experimental procedure

The source of chirped microwave pulses

In order to produce a chirped microwave pulse we are using two different frequency synthesizers. One of those generators produces is amplitude modulated (AM), the other one is frequency modulated (FM). Both signals are mixed and amplified (see Fig. 3.8) and sent to antenna close to the trapped atoms. We operate the AM generator at 10.2 GHz and the FM generator at 1 GHz, so that the output radiation, coming out from microwave antenna has a frequency of 9.2 GHz (see Fig. 3.8).
As a source of 10.2 GHz we use the synthesizer ("Agilent",8375A). It generates the frequencies up to 20 GHz with the sub-Hertz accuracy, provided that it is locked to an external 10 MHz rubidium frequency standard (Stanford Research Systems, PRS10). It can be operated in the amplitude modulation mode. In this mode the output power is controlled by an external signal, whose input voltage of (-10,10) V is proportional to the logarithmic output power. In order to generate the microwave pulse, we use this external signal with a special profile, which compensates the nonlinear response of the amplifier so, that the output microwave radiation from the antenna has the desired properties.

The second synthesizer, ("Rohde&Schwarz", SML02), is used for externally controlled frequency modulation. Its output frequency is the sum of the fixed
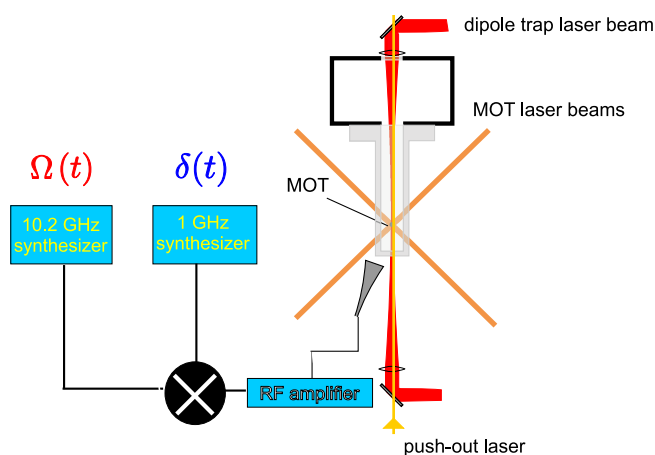
Figure 3.8: Setup of microwave source.

frequency ν_0, which we set to 1 GHz and the frequency ν_{off}, which is proportional to the control voltage.

Both synthesizer signals are sent to a frequency mixer ("MITEQ", MO812). The output signal of this mixer is a signal with a frequencies, equal to the sum and the difference of the frequencies of the input signals. The output of the mixer is sent to a power amplifier (Industrial Electronics, AM53-9-9.4-33-35), which amplifies the microwave signal at 9.2 GHz by 36 dB. It can deliver a maximum output power of +36 dBm. The output signal from the mixer at 11.2 GHz is not amplified, since its frequency lies far out of the amplifier bandwidth. The power amplifier is connected to a dipole antenna.

So, our frequency synthesizers together with the mixer and the amplifier are playing a role of a transfer function between the external signals, which control the AM and FM synthesizers, respectively, and the microwave pulse, generated by the antenna.

The pumping and repumping laser beam

In order to pump the trapped atoms in the outermost Zeeman sublevel of the $F = 4$ hyperfine state two separate laser beams are used in our setup. The pumping laser is locked to the $F = 4 \longrightarrow F = 3/5$ crossover and is σ^+ polarized. This transition is blue detuned by 25 MHz with respect to the transition $F = 4 \longrightarrow F' = 4$ of the free atom. This blue detuning is compensated by the blue detuning of the corresponding transition by the dipole trap, so that this laser almost resonant with $F = 4 \longrightarrow F' = 4$ transition of the trapped atom and pumps the atom into the

dark state $|F = 4, m_F = 4\rangle$.

Atom, excited in the state $F' = 4$ can decay into $F = 3$ state. In order to bring the atom back into the pumping cycle an additional repumping laser beam is applied during the pumping process. It is resonant with the $F = 3 \longrightarrow F' = 4$ transition and has a σ^+ polarization.

Magnetic field configuration

In order to have a well-defined quantization axis during the optical pumping and push-out processes, stray magnetic field, Earth magnetic field and a field from the surrounding devices should be compensated. Three orthogonal pairs of magnetic coils, placed around the vacuum cell, are used for this purpose. In addition, one of those pairs of coils is used to produce a guiding field to provide a quantization axis for the optical pumping.

State selective detection and push-out laser

For manipulation of hyperfine states it is essential to have their efficient detection. In our experiment, for those purposes, we use a so-called push-out laser.

This laser is locked to the $F = 4 \longrightarrow F' = 5$ transition, and its application expels the atoms in the hyperfine state $F = 4$ out of the dipole trap, leaving the atoms in the state $F = 3$ unaffected. It is shined in parallel to the optical axis of the dipole trap and has σ^+-polarization. The atoms, exposed to the σ-polarized radiation of this frequency, after several scattering events, undergoes the closed transition $|F = 4, m_F = 4\rangle \longleftrightarrow |F = 5, m_F = 5\rangle$ (in the case of σ^+-polarized light). Since the push-out laser is never perfectly σ-polarized, there is a finite probability of the following process: a π-polarized photon off-resonantly excites the atom in the state $|F = 4\rangle$, then the atom spontaneously decays in $F = 3$ hyperfine state, which is dark for the push-out laser beam. In order to decrease the probability of this process, the number of photons scattered by the atom, before it leaves the trap should be minimal. Hence it is important to push the atoms out of the trap, rather than to heat them out. Indeed, if the pressure, induced by the "push-out" laser is weaker than the dipole force, the atom is "heated up" by recoil-heating [SUT97], and on average increases its energy by twice the recoil energy per scattered photon $E = \frac{\hbar^2 k^2}{M_{\text{Cs}}}$. The number of photons needed to *boil* the atom out of the dipole trap in this case is determined by the condition:

$$U_0 = n_{boil} E = n_{boil} \frac{\hbar^2 k^2}{M_{\text{Cs}}} \qquad (3.23)$$

In contrast, if the radiation pressure force is stronger then the opposing dipole force, then the heating mechanism is qualitatively different, and the absorbed momenta of the "push-out" beam photons will add up. Thus the number of photons, required for atom to leave is defined by the following equation:

$$U_0 = \frac{n_{push}^2}{2} \frac{\hbar^2 k^2}{M_{Cs}} \tag{3.24}$$

Hence, comparing (3.23) and (3.24), one obtains $n_{push} = \sqrt{2n_{boil}}$. For $U_0 = 1$ mK n_{boil}=5000 and n_{push}=100.

An experimental sequence, used to verify the efficiency of state-selective detection is presented on the Fig. 3.9.

Less then 1 % of the loaded atoms, prepared in the $F = 4$ state survive the push-out process. As a counter check, the survival probability of the atoms, prepared in the state $F = 3$ is measured (lower graph). In Fig. 3.9 this survival probability is 95%, and it can be (in the case of optimal alignment) as high as 99%. Initial preparation of the atoms in one or the other hyperfine state is accomplished by optical pumping. For this purpose, we switch off cooling or repumping laser beam later than the other laser beam. Indeed, hyperfine state $F = 3$ ($F = 4$) is the dark state for the cooling (repumping) laser.

Experimental procedure

In order to accumulate experimental data within a reasonable amount of time, the experiment is realized by repetitive running of a series of almost identical sequences. Each sequence defines a complete set of analog and digital signals, controlling in parallel the set of devices, constituting our experimental setup. All experimental results, described in the present section rely on the comparison of the initial number of atoms (their number just before the loading into the dipole trap) and their final number (their number after intermediate experiments and their transfer from the dipole trap to the MOT). The number of atoms is inferred from the fluorescence, translated to the signal, coming from the APD.

As an example the timing procedure that we use for the experimental realization of adiabatic passages is given below Fig. 3.10.

1) As a first step of the experiment atoms are loaded from the background gas into the MOT. In order to do this, the MOT capture cross section is increased and after atoms are loaded, the MOT is compressed back. This is achieved by decreasing and increasing the quadrupole magnetic field gradient, respectively. The variation
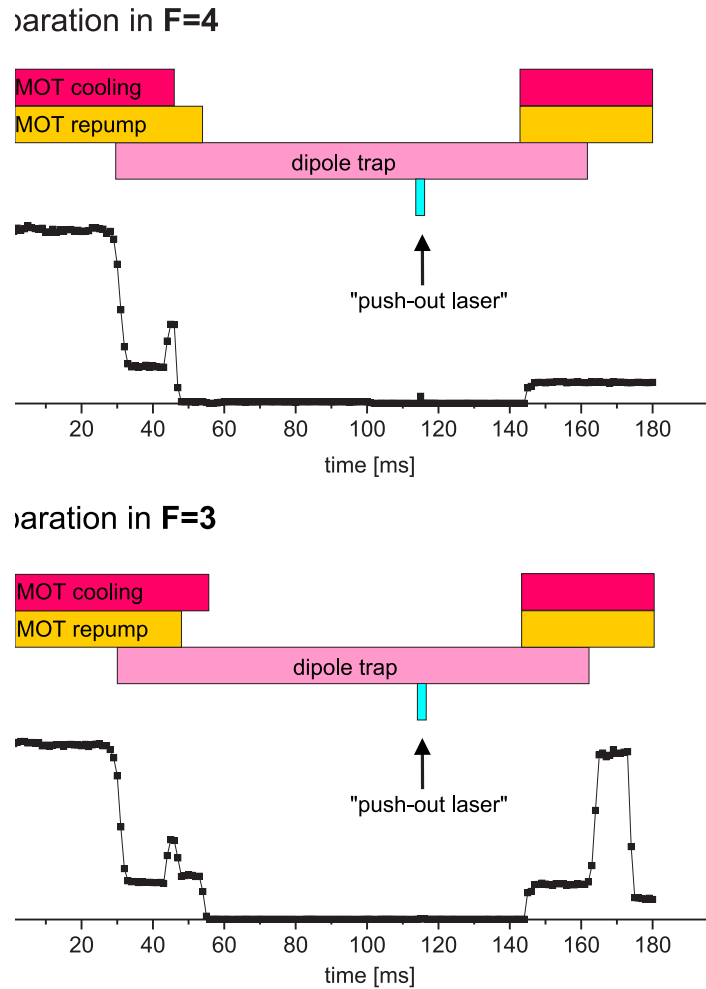
Figure 3.9: Scheme of state selective detection. The presented signal is the sum
of fluorescence signals from 10 identical experiments, corresponding
to the fluorescence signal of around 200 atoms. Push-out laser ex-
pels more than 95% of the atoms, prepared in $F = 4$. The atoms,
prepared in the $F = 3$ survive application with 95% probability.

of the duration of low magnetic field gradient results in the variation of the number
of captured atoms. By decreasing (increasing) the time of the low magnetic field
gradient MOT captures less (more) atoms.

2) As a next step, atoms trapped in the MOT are transferred to the dipole trap.
In order to cool the atoms deep into the dipole trap potential wells, the parameters
of the MOT (detuning and power) are set to the optimal parameters (see Chapter
2) during the transfer. In order to transfer trapped atoms in the dark state $F = 4$,
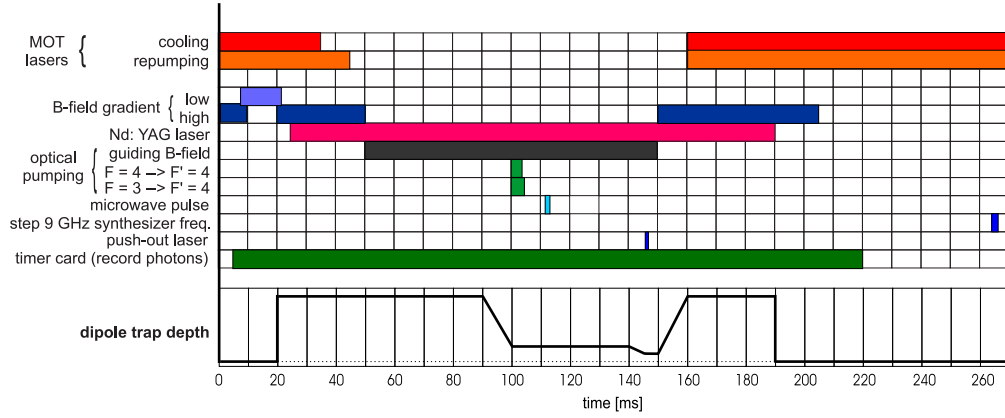
Figure 3.10: the timing sequence.

repumping laser beam is left on a little longer than cooling laser beam.

3) After atoms are transferred into the dipole trap the optical pumping into the outermost Zeeman sublevel has to be carry out. This is achieved by shining on the site of the MOT both pumping and repumping laser beams (See previous section). In order to have a well-defined quantization axis the guiding magnetic field along the dipole trap is applied during the pumping (See fig. 3.11).
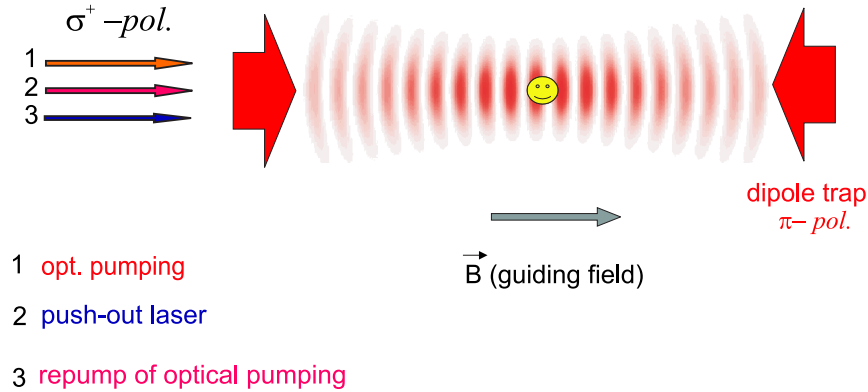
Figure 3.11: Configuration of the pumping laser beams.

4) The atoms in the state $|F = 4, m_F = 4\rangle$ are then exposed to the chirped microwave pulse of the form, given in (3.20). In order to induce only the transition $|F = 4, m_F = 4\rangle \longleftrightarrow |F = 3, m_F = 3\rangle$ a splitting larger than $2\delta_m$ (in this case of the order of 300 kHz) between Zeeman sublevels is required. This is achieved by

applying an offset magnetic field of 2 G along the dipole trap axis, which results in about 700 kHz splitting between neighboring Zeeman transitions.

5) In order to detect the hyperfine state after exposing atoms to the microwave radiation the push-out laser is shined along the dipole trap, which expels all atoms in the state $F = 4$ out of the dipole trap. To have a well-define direction of the quantization axis during push-out process, the guiding magnetic field is applied along the optical axis of the dipole trap. During the application of the push-out laser the dipole trap is lowered, approximately by a factor of 10. This has to be done to insure that the radiation pressure force of the push-out laser is stronger than the dipole force. Because during the lowering of the dipole trap the m_F states can mix due to Raman transitions, the lowering of the dipole trap should be done before pumping the atoms in the outermost Zeeman sublevel.

6) The information, providing the efficiency of the population transfer is the *initial* and *final* number of atoms, under the assumption that a large statistics is collected. The *initial* number of atoms is their amount before the transfer to the dipole trap took place. The *final* number of atoms is their amount after performance of the intermediate experiments in the dipole trap have taken place, and they transferred back to the MOT.

7) In the end of each experiment the external signal steps the frequency of the Agilent and the same experimental procedure is repeated automatically. This allows as to perform the measurement of the whole spectrum automatically.

3.3.2   Results and conclusions

Rabi oscillations

As a first step we measured the Rabi oscillations between $|F = 4, m_F = 4\rangle \longleftrightarrow |F = 3, m_F = 3\rangle$ transition. In order to measure Rabi frequency we have to follow a procedure, described in the previous section. Here, to manipulate the population of hyperfine states we applied the resonant microwave radiation of varied duration. In Fig. 3.12 the population transfer a function of duration of resonant microwave radiation is presented. Each point on the spectrum is the result of the experiment with 150 atoms on average. Measured dependency was fitted with the function $y = y_0 + A \sin(\frac{1}{2}\Omega t)^2$. The obtained Rabi frequency is equal to $\Omega = 2\pi \times (13.5 \pm 0.07)$ kHz. The contrast of the presented oscillations is perfect and is close to 100%. The efficiency of population transfer reaches only 60 %, which is determined by the atom losses during the experiment.

The sources of the atom losses are: the transfer efficiency from the dipole trap to the MOT, the loss of atoms due to optical pumping, the imperfect pumping in the the outermost Zeeman sublevel, inperfection of the push-out laser and the loss of atoms due to cold collisions. The last source is the dominating loss mechanism, since we were working with the large number of atoms. Following consideration explain shortly the effect of cold collisions: suppose that two or more atoms are localized in the single potential well. Assume, that one of those atoms is in the energetically higher hyperfine state $F = 4$. The atoms then with certain probability can undergo inelastic collision, where their internal energy will be converted into the kinetic energy, far exceeding the dipole trap potential depth and both atoms escape the dipole trap in this process.
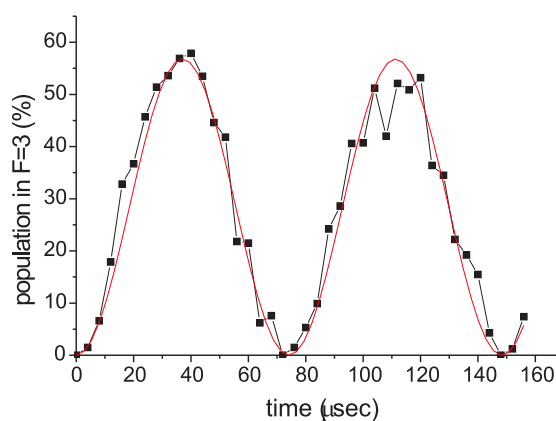
Figure 3.12: Rabi oscillations between $|F = 4, m_{\mathrm{F}} = 4\rangle$ and $|F = 3, m_{\mathrm{F}} = 3\rangle$ states. The data points are fitted with $y = y_0 + A \sin(\frac{1}{2}\,\Omega\,t)^2$. The inferred Rabi frequency is equal to the $2\pi \times (13.5 \pm 0.07)$ kHz.

Adiabatic passage

To measure the spectrum of population transfer via adiabatic passages we use the following parameters:

$$
\begin{aligned}
\Omega_{\mathrm{m}} &= 2\pi \times 13.5 \text{ MHz} \\
\delta_{\mathrm{m}} &= 140 \text{ kHz} \\
t_0 &= 2 \text{ ms}
\end{aligned}
$$

The measured population transfer is presented in Fig. 3.13. Each point of the above given dependency is the result of experiments with approximately 100 atoms,

distributed over three independent trials. Each point was measured, applying the adiabatic passage with the corresponding frequency chirp offset. The frequency chirp offset was stepped over the region of approximately 400 kHz with step size of 2 kHz, symmetrical with respect to $\delta_0 = 0$.
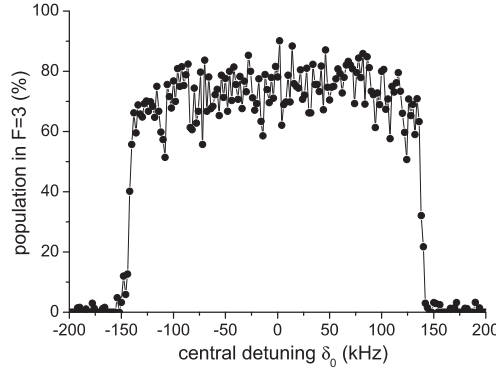
**Figure 3.13**: The measured population in the state $F = 3$ after the application of the chirped microwave pulse. The population transfer has an expected plateau-like form. The efficiency reaches only 75%, which is determined by the loss mechanisms in connection with a large number of atoms.

The spectrum has an expected plateau-like form. The plateau width is approximately $2\delta_\mathrm{m}$. The measured transfer efficiency agrees well with numerically calculated one (see Fig. 3.6).

The frequency region, which corresponds to the rise of the efficiency from zero to its maximum is approximately equal to 20 kHz. This value agrees well with the corresponding numerically calculated rise region. The plateau, as expected, is symmetrical with respect to the atomic resonance at $\delta_0 = 0$. The population transfer efficiency rises only up to 75 % level. This is not a limitation of the adiabatic passages technique, but is determined by the loss mechanisms during the experiment (see above). Here, in contrast to the Rabi frequency measurement, we load less atoms in each sequence, which reduces the loss down to about 24%. We check these losses in a separate measurement. The Figure 3.13 is one of the spectra, recorded via the adiabatic passages.

The measured spectra indicate that the adiabatic passage induce a population transfer between hyperfine states of Cs atoms with an efficiency close to 100 %, taking into account the losses due to our detection scheme. The measured spectrum has an expected plateau-like form. As a possible application, the technique of the adiabatic passages can be used to induce position-dependent population transfer of the atoms,

confined in the dipole trap. Indeed, this application has been realized and discussed in the next chapter.

Chapter 4

Addressing of individual atoms

Whereas addressing of single ions has been realized by now [NAE99], addressing of individual neutral atoms remained until most recently an open problem in the field of engineering with single atoms.

Combining the ability to determine the absolute atomic position and the method of adiabatic passages, the internal state manipulation of individual atoms was achieved in our experiment, which is the subject of this chapter.

4.1 Adiabatic passage in a magnetic field gradient

In the previous chapter I concentrated on adiabatic passages between the states of a two-level system with fixed transition frequency.

Using the method of adiabatic passages we want to position-dependently manipulate the internal states of the individual atoms. Since we cannot focus the microwave radiation, we are working with the magnetic field sensitive outermost Zeeman transition ($|F = 4, m_\mathrm{F} = 4\rangle \longleftrightarrow |F = 3, m_\mathrm{F} = 3\rangle$) (see Fig. 4.1). By applying a magnetic field gradient along the dipole trap axis the frequency of the $|F = 4, m_\mathrm{F} = 4\rangle \longleftrightarrow |F = 3, m_\mathrm{F} = 3\rangle$ transition becomes position-dependent. For this purpose we use the MOT coils, which produce a quadrupole magnetic field, whose magnitude linearly increases from its center.

4.1.1 Adiabatic passage with oscillating atoms

The atoms stored in the dipole trap oscillate in the corresponding potential wells. Since the quadrupole magnetic field raises linearly in all directions, and since the atomic resonance frequency is magnetic field dependent, oscillations of the atoms in both radial (transverse to the trap axis) at frequency ω_rad and axial (along the
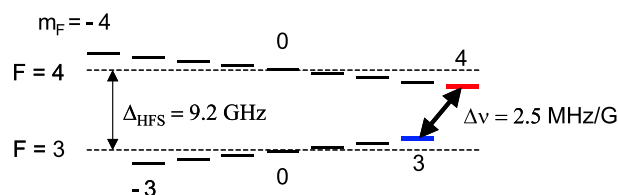
Figure 4.1: Zeeman splitting of the Cs hyperfine ground states.

trap axis) directions at frequency ω_{ax} result in an oscillation of the atomic resonance frequency. Thus the effective detuning of the applied microwave radiation has the following form:

$$\delta(t) = \delta_0 - \delta_{\text{m}} \cos\left(t\,\frac{\pi}{t_0}\right) + a_{\text{rad}} \sin(\omega_{\text{rad}}t) + a_{\text{ax}} \sin(\omega_{\text{ax}}t). \qquad (4.1)$$

Here, the first term, δ_0, is the frequency chirp offset, the second term is the frequency modulation of the microwave radiation necessary for adiabatic passages (see Eq. 3.20). The last two terms describe the modulation of the atomic resonance frequency due to radial and axial oscillations in the trap.

The frequencies of axial and radial oscillations of an atom in the dipole trap of depth $U_0 = 1$ mK are about 230 kHz and 3 kHz, respectively, and are proportional to $U_0^{1/2}$. The fast axial oscillations with a small spatial amplitude result in the fast oscillation of the detuning with a small frequency amplitude a_{ax}. The Bloch vector, oscillating around the torque vector sees the averaged position of the torque vector, provided that the frequency of the axial oscillations is larger than the instantaneous value of the effective Rabi frequency ($\omega_{\text{ax}} > |\mathbf{\Omega}_{\text{eff}}|$). Hence, the axial oscillation do not influence the dynamics of the Bloch vector. Remarkably, in the condition of the adiabaticity (see Eq. 4.4) the time derivative of the rapidly oscillating detuning $\dot{\delta}$ should be averaged over the time of the order of $1/|\mathbf{\Omega}_{\text{eff}}|$. The rapidly oscillating part averages out and the Bloch vector following stays undisturbed.

However, the frequency of the radial oscillations is smaller than $|\mathbf{\Omega}_{\text{eff}}|$. Thus, they affect the dynamics of the Bloch vector during the passage and reduce its adiabaticity.

The atoms, loaded from the MOT to the dipole trap, are localized in the vicinity of the zero point of the magnetic field. There the magnetic field gradient in the radial direction is maximal, and thus the amplitude of radial oscillation results in a maximal amplitude of the transition frequency oscillation. In order to reduce the magnetic field gradient seen by the atom, an offset magnetic field B_{off} is applied along the axial direction of the dipole trap. Illustratively, the application of B_{off} is

equivalent to the displacement from the zero point of a quadrupole magnetic field. Note, that B_{off} does not affect the gradient along the axial direction.

The amplitude of frequency oscillations decrease with the rise of the magnetic field offset according to the following equation:

$$a_{\text{ax}} = \Delta B k \quad = \quad k \left(\sqrt{B_{\text{off}}^2 + B_{\text{rad}}^2} - B_{\text{off}} \right) \tag{4.2}$$

$$= \quad k \left(\sqrt{(B_{\text{off}})^2 + (2B'A_{\text{osc}})^2} - B_{\text{off}} \right) \tag{4.3}$$

Here

$$
\begin{array}{rcl}
a_{\text{ax}} & - & \text{amplitude of frequency oscillations} \\
A_{\text{osc}} & - & \text{spatial amplitude of the radial oscillations} \\
\Delta B & - & \text{amplitude of the magnetic field fluctuations} \\
B_{\text{rad}} & - & \text{magnetic field contribution in the radial direction} \\
\Delta \nu & = & 2.5 \text{ MHz/G}
\end{array}
$$
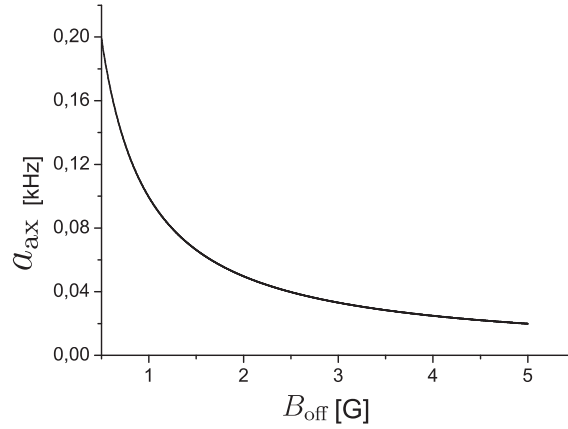
Figure 4.2: The amplitude of the frequency modulation of the atomic resonance frequency in a quadrupole magnetic field decreases for larger offset fields. Shown here is its dependence for a magnetic field gradient of B'=15 G/cm.

The dependency (4.2) is shown in Fig. 4.2. Here, it is assumed that the atoms are always loaded at the site of magnetic field zero-point. From the figure one sees that applying an offset field of the order of few Gauss is sufficient to reduce the effect of the radial oscillations.

4.1.2   Position-dependent population transfer

Application of a linear gradient of a magnetic field along the dipole trap axis results in a position-dependent transition frequency. Hence, the population transfer as a function of the frequency chirp offset (see Fig. 3.13) is mapped into the population transfer as a function of the atomic position and also has a plateau-like form.

The efficiency of the population transfer as a function of position offset was calculated numerically, similar to the numerical simulations of adiabatic passages presented in Sec. 3.2. The chosen set of parameters is the following:

$$
\begin{aligned}
\Omega_{\mathrm{m}} &= 2\pi \times 13.5 \text{ kHz} && \text{- amplitude of the Rabi frequency} \\
\delta_{\mathrm{m}} &= 30 \text{ kHz} && \text{- detuning amplitude of the microwave radiation} \\
t_0 &= 2 \text{ ms} && \text{- interaction duration} \\
A_{\mathrm{rad}} &= 3 \text{ } \mu\text{m} && \text{- amplitude of radial oscillations} \\
\omega_{\mathrm{rad}} &= 2\pi \times 3 \text{ kHz} && \text{- frequency of radial oscillations} \\
B_{\mathrm{off}} &= 4 \text{ G} && \text{- offset magnetic field} \\
B' &= 15 \text{ G/cm} && \text{- magnetic field gradient}
\end{aligned}
$$
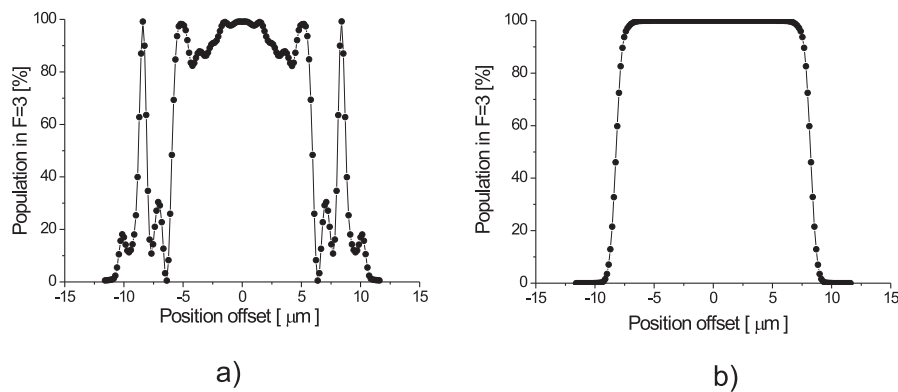
Figure 4.3: Population in F=3 as a function of position offset of the adiabatic passage. a) The offset magnetic field equals to B_{off} =0.02 G. The population transfer does not have a plateau-like form. b) The offset field magnetic field B_{off} =4 G. The population transfer has a plateau-like form.

The population transfer depending on the position is presented in Fig. 4.3 b). It has a plateau-like form. For the chosen parameter, the frequency fluctuation due to

radial atomic oscillations, does not influence the efficiency of the adiabatic passage. The dependency obtained without taking into account the radial oscillations has an identical profile. Thus, for these parameters, the influence of the radial oscillations is negligible.

In Fig. 4.3 a) the efficiency of population transfer is shown if the offset magnetic field B_{off} is reduced to 0.02 G. This efficiency does not have a plateau-like profile and cannot be used for addressing. The origin of the deviation from the plateau-like form is the following. As long as we reduce the B_{off} the magnetic field gradient increases, and as a consequence the amplitude of the frequency oscillations also increases. And the Bloch vector cannot perfectly follow the torque vector, and thus the population transfer drops.

4.2 Experimental realization

Combining the position-dependent popualtion transfer with the ability to resolve individual atoms in space, we realize the individual addressing of the stored atoms.

4.2.1 Loading atoms

As it was pointed out in Chapter 2, the size of the MOT is of the order of 10 μm. During the transfer of atoms from the MOT into the dipole trap, atoms are loaded into random potential wells within the region of the MOT. Taking into account that we can optically resolve two atoms which are more than 2.7 μm apart, the probability is small to have several atoms in the dipole trap with sufficient spacing that they can all be resolved. In order to create a chain of well-resolved single atoms we perform the following procedure. After atoms are loaded into the dipole trap, we switch the trap configuration from standing-wave to running-wave by switching off one of the trap laser beams. This eliminates the axial confinement of the atoms and, since their kinetic energies are, in general, different, they start to spread along the trap axis. After one ms the separation between the atoms is usually large enough to resolve them. By switching on both laser beams, the atoms are recaptured in the standing wave dipole trap.

4.2.2 Frequency calibration

To address atoms in the magnetic field gradient, we have to know the exact correspondence between an atomic position (i. e. CCD pixels where the atom is detected)

and the atomic transition frequency in the presence of the magnetic field gradient and magnetic offset field. To measure this correspondence we perform the following calibration procedure. We first load a large number of atoms into the dipole trap and prepare them in the state $|F = 4, m_\mathrm{F} = 4\rangle$. After that, we apply an adiabatic passage with some frequency chirp offset δ_0. Then we apply the push-out laser and measure the position along the dipole trap where atoms have survived. This position corresponds to the transition frequency resonant to the applied microwave radiation. We perform this measurement for several different values of δ_0. Later, this obtained dependance will help us to determine the resonance frequency of any resolved atom.

4.2.3 Addressing a selected atom

To address a selected atom out of the chain of atoms stored in the dipole trap we follow the experimental procedure used for adiabatic passages and described in Sec. 3.3.1 but with some modifications. Here the experimental procedure is the following:

1) First, we load several atom into the dipole trap, illuminate them with the optical molasses, and take an image. Determining the positions of the atoms we extract the information about the frequency of the $|F = 4, m_\mathrm{F} = 4\rangle \longleftrightarrow |F = 3, m_\mathrm{F} = 3\rangle$ transition for each individual atom.

2) Then, we optically pump trapped atoms into the outermost Zeeman sublevel $|F = 4, m_\mathrm{F} = 4\rangle$. During the pumping the atoms do not change their position in the trap. This can separately be checked by comparing their positions before and after the optical pumping.

3) Next, we apply an adiabatic frequency chirp through the resonance of a selected atom.

4) In order to keep only those atoms trapped which have changed their hyperfine state after the application of the microwave radiation we apply the push-out laser.

5) To check that the selected atom is still in the dipole trap, we take a second image with the CCD camera.

Examples of the addressing of the central atom out of a chain of three well-resolved atoms are presented in Fig. 4.4. The first picture shows a chain of trapped atoms before the application of the microwave pulse. The second picture shows the image of the atoms, which remain trapped after the application of the push-out laser beam. Each time, out of the chain of the three trapped atoms the population of the middle

one is transferred.
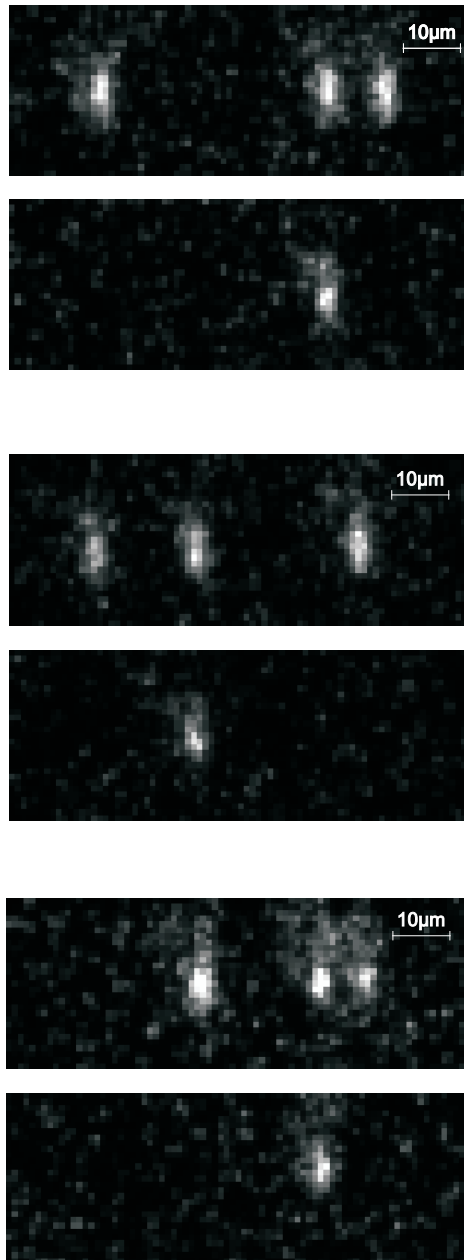
Figure 4.4: Three examples of addressing individual atoms. The first picture shows three atoms loaded in the dipole trap. The adiabatic passage is applied to the middle atom. The second picture is taken after application of the push-out laser and illustrates the addressing of the middle atom.

4.2.4 Characterization of addressing

To quantitatively characterize the addressing we have to measure the efficiency of population transfer and its spatial resolution.

The experimental procedure is similar to the one explained in the previous section. For this measurement the loading time of the MOT is reduced in order to trap on average one atom per shot. Of course, the number of loaded atoms is governed by the Poissonian statistics, and only in about 30% of the cases we have initially one atom trapped in the MOT. All trials, where the initial number of atoms is different from one, are dismissed afterwards. To measure the position of the trapped atom, we take its image. Then we apply a chirped microwave pulse with δ_0, corresponding to a defined distance d_{off} from the atom. After application of the push-out laser we detect the presence of the atom in the dipole trap by transferring it back into the MOT. For each d_{off} we repeat the measurement many times to get better statistics.

The efficiency of a single atom population transfer as a function of the position offset of δ_0 was measured for the following experimental parameters:

$$
\begin{aligned}
\Omega_{\text{m}} &= 2\pi \times 13.5 \text{ mHz} \\
\delta_{\text{max}} &= 30 \text{ kHz} \\
t_0 &= 2 \text{ ms} \\
B_{\text{off}} &= 4 \text{ G} \\
B' &= 15 \text{ G/cm} \sim (3.8 \text{ kHz}/\mu\text{m})
\end{aligned}
$$

The measured efficiency is presented in Fig. 4.5. The population transfer reaches 97 % at $\delta_0 = 0$ and completely vanishes at $d_{\text{min}} = 12~\mu\text{m}$. This means, that if two atoms are separated by more than d_{min}, we can invert the population of one atom with an efficiency close to 100% without affecting the other atom. Note, that the number 97% is the efficiency of the whole experiment including all intermediate steps: transfer of the atom from the MOT into the dipole trap, optical pumping, population transfer with adiabatic passages, application of the push-out laser beam and transfer back into the MOT.

The falling edges of the measured spectrum are not as steep as expected from the numerically calculated one (see Fig. 4.3 b). This is determined by fluctuations of the magnetic offset field. These fluctuations result in a fluctuation of the detuning and as a result reduce the adiabaticity of the passage.

It is desirable to increase the resolution of the population transfer spectrum. This is possible, in principle, by decreasing the amplitude of the frequency chirp. However,

we found that in this case the maximum efficiency of population transfer drops. By suppressing the magnetic field fluctuations we should be able to increase the coherence time and thus to sharpen the edges of the spectrum. Then it will be possible to reduce the amplitude of the frequency chirp further without loss of transfer efficiency.
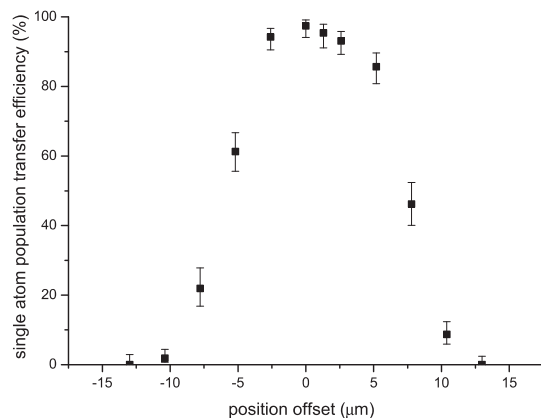

Figure 4.5: Efficiency of a single atom population transfer versus position offset of the frequency chirp. The efficiency reaches 97% at the site of the atom and drops to zero at a distance of 12 μm.

Summary

Quantum information processing is a growing field of modern physics. It has a range of possible applications - it can be used for studying decoherence of quantum systems, for quantum cryptography and quantum computation. To implement quantum information processing several experimental tasks should be accomplished. First of all, the two-level quantum systems, used for carrying the quantum information should be decoupled from the environment, because decoherence would destroy the interferences that constitute the quantum computation. The second requirement for a realization of quantum algorithms is the ability to independently manipulate the state of each individual two-level system. One of the possible candidates, which can be used for implementation two-level quantum systems nowadays are ions and neutral atoms. Whereas the addressing of trapped ions has been realized by now [NAE99], the addressing of individual neutral atoms remained until most recently an open problem in the field of engineering with single atoms.

During my diploma thesis such an addressing of individual atoms in an optical dipole trap was demonstrated. In order to achieve this task we had to develop versatile and advanced tools.

First of all, we demonstrated a non-destructive imaging of individual atoms in the dipole trap, which is a new technological achievement in engineering with systems of neutral atoms. Furthermore, during my thesis I carried out a characterization of a recently implemented intensified CCD camera, which provides a spatial information of the trapped atoms. We determined optimal parameters for continuous observation and cooling of atoms in the trap. This now enables us to resolve individual atoms in the standing wave dipole trap and provides a resolution of 400 nm.

Furthermore, we implemented adiabatic passages between the hyperfine ground states, using microwave radiation. This constitutes a robust method for population transfer. As a preliminary work for this achievement I performed extensive theoretical simulations to determine suitable parameters for our setup.

The application of a magnetic field gradient along the optical axis results in position dependent transition frequency of the outermost Zeeman sublevels of the hyperfine states. Combining the ability to determine the absolute atomic position and the method of adiabatic passages, we achieved a manipulation of individual atoms. At the present moment, we can address a priori chosen individual atom within a chain of atoms with a negligible effect on the neighboring atoms, given that the atoms are situated more than 12 μm apart.

Bibliography

[ALL75]   L. ALLEN AND J. H. EBERLY, *Optical resonance and two-level atoms*, Wiley, New York (1975)

[ALT03]   W. ALT, D. SCHRADER, S. KUHR, M. MÜLLER, V. GOMER AND D. MESCHEDE, *Properties of single atoms in an optical dipole trap*, Phys. Rev. A **67**, p. 033403 (2003)

[ASK62]   G. A. ASKAR'YAN, Zh. Eksp. Teor. Fiz. **42**, p. 1567, engl. translation Sov. Phys. JETP **15**, 1088 (1962)

[BAL85]   V. I. BALYKIN, V. S. LETOKHOV, V. G. MINOGIN, Y. V. ROZHDESTVEN-SKY AND A. I. SIDOROV, *Radiative collimation of atomic beams through two-dimensional cooling of atoms by laser-radiation pressure*, J. Opt. Soc. Am. B **2**, p. 1776–1783 (1985)

[BJO78]   J. E. BJORKHOLM, R. FREEMAN, A. ASHKIN AND D. B. PEARSON, *Observation of Focusing of Neutral Atoms by the Dipole Forces of Resonance-Radiation Pressure*, Phys. Rev. Lett. **41**, p. 1361 (1978)

[BOH86]   A. BOHM, *Quantum mehanics*, Springer, New York (1986)

[CHU85]   S. CHU, J. E. BJORKHOLM, A. CABLE AND A. ASCHKIN, *Three-dimensional viscous confinement and cooling of atoms by resonance radiation pressure*, Phys. Rev. Lett. **55**, p. 48–51 (1985)

[CHU86]   S. CHU, J. E. BJORKHOLM, A. ASHKIN AND A. CABLE, *Experimental observation of optically trapped atoms*, Phys. Rev. Lett. **57**, p. 314 (1986)

[CHU98]   I. L. CHUANG, L. M. K. VANDERSYPEN, X. ZHOU, D. W. LEUNG AND S. LLOYD, *Experimental realization of a quantum algorithm*, Nature **393**, p. 143 (1998)

[COH92]   C. COHEN-TANNOUDJI, J. DUPONT-ROC AND G. GRYNBERG, *Atom-Photon Interactions*, Wiley, New York (1992)

[GRI73]   M. D. GRISP, *Adiabatic-following approximation*, Phys. Rev. A **8**, p. 2128–2135 (1973)

[Gri00]   R. Grimm, M. Weidemüller and Y. Ovchinnikov, *Optical dipole traps for neutral atoms*, Adv. At. Mol. Opt. Phys. **42**, p. 95 (2000)

[Gue02]   S. Guerin, S. Thomas and H.Jauslin, *Optimization of population transfer by adiabatic passage*, Phys. Rev. A **65**, p. 023409 (2002)

[Gul03]   S. Gulde, M. Riebe, G. P. T. Lancaster, C. Becher, J. Eschner, H. Häffner, F. Schmidt-Kaler, I. L. Chuang and R. Blatt, *Implementing the Deutsch-Jozsa algorithm on an ion-trap quantum computer*, Nature **421**, p. 48 (2003)

[Hän75]   T. W. Hänsch and A. Schawlow, *Cooling of Gases by Laser Radiation*, Opt. Commun. **13**, p. 68 (1975)

[Hau96]   D. Haubrich, H. Schadwinkel, F. Strauch, B. Ueberholz, R. Wynands and D. Meschede, *Observation of individual neutral atoms in magnetic and magneto-optical traps*, Europhys. Lett. **34**, p. 663 (1996)

[Jac62]   J. D. Jackson, *Classical Electrodynamics*, Wiley, New York, second edition (1962)

[Kuh01]   S. Kuhr, W. Alt, D. Schrader, M. Mueller, V. Gomer and D. Meschede, *Deterministic Delivery of a Single Atom*, Science **293**, p. 278–280 (2001)

[Kuh03]   S. Kuhr, W. Alt, D. Schrader, I. Dotsenko, Y. Miroshnychenko, W. Rosenfeld, M. Khudaverdyan, V. Gomer, A. Rauschenbeutel and D. Meschede, *Coherence properties and quantum state transportation in an optical conveyor belt*, accepted for publication in Phys. Rev. Lett. (2003)

[Let77]   V. S. Letokhov, Minogin and Pavlik, Zh. Eksp. Teor. Fiz. **72**, p. 1382, engl. translation JETP Lett. **45**, 698 (1977)

[Lou83]   R. Loudon, *The Quantum Theory of Light*, Clarendon, Oxford (1983)

[Mak01]   Y. Maklin, G. Schön and A. Shnirman, *Quantum-state engineering with Josephson-junction devices*, Rev. Mod. Phys. **73**, p. 357 (2001)

[Mes65]   A. Messiah, *Quantum Mechanics*, Amsterdam (1965)

[Met99]   H. J. Metcalf and P. van der Straten, *Laser Cooling and Trapping*, Springer, New York (1999)

[Mir02]   Y. Miroshnychenko, *Design and test of a high finesse resonator for single atom experiments*, master thesis, Universität Bonn (2002)

[Mon95]   C. Monroe, D. M. Meekhof, B. E. King, S. R. Jefferts, W. M. Itano, D. J. Wineland and P. Gould, *Resolved-Sideband Raman Cooling of a Bound Atom at the 3D Zero-Point Energy*, Phys. Rev. Lett. **75**(22), p. 4011–4014 (1995)

[Nae99]   H. C. Naegerl, D. Leibfried, H. Rohde, G. Thalhammer, J. Eschner, F. Schmidt-Kaler and R. Blatt, *Laser addressing of individual ions in a linear ion trap*, Phys. Rev. A **60**, p. 145–148 (1999)

[Pet02]   C. J. Pethick and H. Smith, *Bose-Einstein Condensation in Dilute Gases*, Cambridge University Press (2002)

[Pri]   Princeton Instruments, *Manual.PTG Programmable Timing Generator*

[Ric00]   K. T. Rickes, L. P. Yatsenko, S. Steuerwald, T. Halfmann, B. W. Shore and N. V. Vitanov, *Efficient adiabatic population transfer by two-photon excitation assisted by a laser-induced Stark shift*, Jour. of Chem. Phys. **113**, p. 534–546 (2000)

[Ros03]   W. Rosenfeld, *A high finesse optical resonator for cavity QED experiments*, master thesis, Universität Bonn (2003)

[San02]   C. Santori, D. Fattal, J. Vukovi, G. S. Solomon and Y. Yamamoto, *Indistinguishable photons from a single-photon device*, Nature **419**, p. 594 (2002)

[Sch00]   D. Schrader, *Ein Förderband fuer einzelne Atome*, master thesis, Universität Bonn (2000)

[Sch01a] N. Schlosser, G. Reymond, I. Protsenko and P. Grangier, *Sub-Poissonian loading of single atoms in a microscopic dipole trap*, Nature **411**, p. 1024 (2001)

[Sch01b] D. Schrader, S. Kuhr, W. Alt, M. Müller, V. Gomer and D. Meschede, *An Optical Conveyor Belt for Single Neutral Atoms*, Appl. Phys. B **73**, p. 819 (2001)

[Sho90]   B. W. Shore, *The Theory of Coherent Atomic Excitation*, Wiley (1990)

[Sho97]   P. Shor, *Polynomial-time algorithms for prime factorization and discrete logarithms on a quantum computer*, SIAM J. Comp. **26**, p. 1484 (1997)

[Sut97]   D. Suter, *The physics of Laser-Atom Ineractions*, Cambridge University Press, Cambridge (1997)

[Win75]   D. Wineland and H. Dehmelt, *Proposed $10^{14}\Delta\nu < \nu$ Laser Fluorescence Spectroscopy on Tl^+ Mono-Ion Oscillator III (side band cooling)*, Bull. Am. Phys. Soc. **20**, p. 637 (1975)

Acknowledgements

In only few hours time a my year-long diploma thesis will get over, and at this both solemn and sad moment I want to express my acknowledgements to those people, with whom I had a pleasure to spend this final year of my undergraduate studies:

First of all I would like to express my acknowledgements to my supervisor — Prof. D. Meschede for providing me access to this wonderful experiment.

I would like to thank Prof. I. Brock for taking the role of a coreferent.

I want to thank the single atom crew for teaching me so much stuff — it was a really fruitful time!

I want to thank Dominik Schrader for his endless patience and willingness always to encourage me,

Wolfgang Alt - who always found a simple answer to any of my questions,

Igor Dotsenko and Yevhen Miroschnichenko for having a nice time all through this year and helping me in all aspects,

Stefan Kuhr for his endless optimism and enthusiasm,

Wenjamin Rosenfeld for his unique sense of humor,

Arno Rauschenbeutel for his willingness to lead any discussion in friendly atmosphere.

I want to sincerely thank to all members of this group,

I want to thank my parents who always supported me in any aspects and encouraged me in taking all my steps.

Erklärung

Ich versichere, daß ich diese Arbeit selbständig verfaßt und keine
anderen als die angegebenen Quellen und Hilfsmittel benutzt sowie
Zitate kenntlich gemacht habe.

Bonn, im November 2003